AD

REPORT NO. RE-TR-72-9

DIGITAL SIMULATION OF MONOPULSE ANGLE TRACKING WITH MULTIPATH PROPAGATION

by

Sam O. Dunlap and Bennie E. Pope

May 1972

Approved for public release. Distribution unlimited.

U.S. ARMY MISSILE COMMAND
Redstone Arsenal, Alabama

DISPOSITION INSTRUCTIONS

Destroy this report when it is no longer needed. Do not return it to the originator.

DISCLAIMER

The findings in this report are not to be construed as an official Department of the Army position unless so designated by other authorized documents.

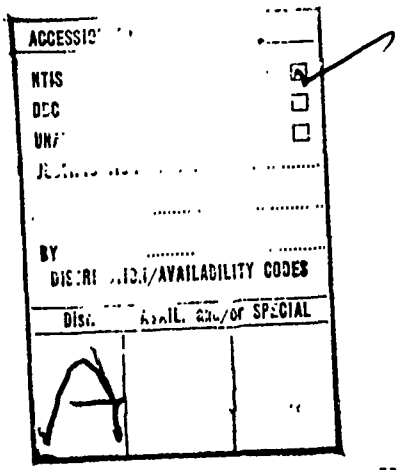

TRADE NAMES

Use of trade names or manufacturers in this report does not constitute an official indorsement or approval of the use of such commercial hardware or software.

UNCLASSIFIED

Security Classification

DOCUMENT CONTROL DATA - R & D

(Security classification of title, body of abstract and indexing annotation must be entered when the overall report is classified)

1. ORIGINATING ACTIVITY (Corporate author)	2a. REPORT SECURITY CLASSIFICATION
Advanced Sensors Directorate Directorate for Research, Development, Engineering and Missile Systems Laboratory U.S. Army Missile Command Redstone Arsenal, Alabama 35809	Unclassified
	2b. GROUP NA

3. REPORT TITLE

DIGITAL SIMULATION OF MONOPULSE ANGLE TRACKING WITH MULTIPATH PROPAGATION

4. DESCRIPTIVE NOTES *(Type of report and inclusive dates)*

Technical Report

5. AUTHOR(S) *(First name, middle initial, last name)*

Sam O. Dunlap
Bennie E. Pope

6. REPORT DATE	7a. TOTAL NO. OF PAGES	7b. NO. OF REFS
31 May 1972	55	4

8a. CONTRACT OR GRANT NO.	9a. ORIGINATOR'S REPORT NUMBER(S)
b. PROJECT NO (DA) 1X263302D212 AMC Management Structure Code No. 523B.12.17100	RE-TR-72-9
c.	9b. OTHER REPORT NO(S) *(Any other numbers that may be assigned this report)* AD
d.	

10. DISTRIBUTION STATEMENT

Approved for public release; distribution unlimited.

11. SUPPLEMENTARY NOTES	12. SPONSORING MILITARY ACTIVITY
None	Same as No. 1

13. ABSTRACT

This report documents recent efforts in digital computer modeling of multipath propagation effects on a modern tracking radar. Specific questions on the role of the earth dielectric constant and surface roughness are considered. Several earth models are also considered, including a flat smooth surface, smooth 4/3 radius spherical surface, and a 4/3 radius spherical earth with rough surface. Two basic scattering models are considered, specular reflection which is coherent in nature and diffuse reflection which is noncoherent.

This study uses a large digital phased array radar simulation which will be described in detail in a future report. The parts of significance to this effort are described for completeness.

DD FORM 1 NOV 68 1473 REPLACES DD FORM 1473, 1 JAN 64, WHICH IS OBSOLETE FOR ARMY USE.

UNCLASSIFIED

Security Classification

14. KEY WORDS	LINK A		LINK B		LINK C	
	ROLE	WT	ROLE	WT	ROLE	WT
Digital computer						
Multipath propagation effects						
Modern tracking radar						
Earth dielectric constant						
Surface roughness						

31 May 1972

Report No. RE-TR-72-9

DIGITAL SIMULATION OF MONOPULSE ANGLE TRACKING WITH MULTIPATH PROPAGATION

by

Sam O. Dunlap and Bennie E. Pope

DA Project No. 1X263302D212

AMC Management Structure Code No. 523B.12.17100

Approved for public release. Distribution unlimited.

Advanced Sensors Directorate

Directorate for Research, Development, Engineering

and Missile Systems Laboratory

U.S. Army Missile Command

Redstone Arsenal, Alabama 35809

ABSTRACT

This report documents recent efforts in digital computer modeling of multipath propagation effects on a modern tracking radar. Specific questions on the role of the earth dielectric constant and surface roughness are considered. Several earth models are also considered, including a flat smooth surface, smooth 4/3 radius spherical surface, and a 4/3 radius spherical earth with rough surface. Two basic scattering models are considered, specular reflection which is coherent in nature and diffuse reflection which is noncoherent.

This study uses a large digital phased array radar simulation which will be described in detail in a future report. The parts of significance to this effort are described for completeness.

CONTENTS

1. Introduction

The main purpose of this report is to document recent multipath propagation studies, particularly, the effects of this phenomenon upon the angle tracking accuracy of a modern tactical radar. The primary goal is to provide a time domain digital simulation of a phased array monopulse tracking radar. To properly exercise this simulation, all input functions must be carefully modeled to provide the proper temporal, amplitude, and phase characteristics. This report develops the multipath component of the input and presents results obtained during verification of the model.

The simulation is described in two parts: multipath models, and target and radar models. The section on multipath develops the several possible components of the multipath signal and illustrates the effect of each component upon the radar. Finally, the composite multipath signal is considered. Sufficient mathematical expressions are included to aid in outlining the approach, and references are given for those interested in the detailed mathematical derivations. Target and radar models are presented only to show how the tracking errors caused by multipath were developed. Details of the radar model will be published in a later report.

This report addresses multipath errors only in the sin β coordinate, which is one dimension of the antenna (sin α, sin β) steering space and corresponds to the elevation coordinate only when sin $\alpha = 0$. For other locations multipath errors exist in the sin α channel also. A cursory examination indicated that these errors would be quite small. Therefore, the simulation runs were normally made for near zero sin α. A very limited number of runs for large sin α steered angle produced sin β error profiles quite similar to those for sin $\alpha = 0$ and sin α multipath errors that were considered insignificant (10^{-3} millisine peaks). Therefore, multipath error in the sin α coordinate was not addressed in great detail.

The results (Paragraph 5) indicate the sensitivity of multipath induced tracking error to two classes of variables; those related to the input and those related to the radar. Input variables of interest are the relative dielectric constant and roughness of the earth surface, the elevation angle of the target, and the target radial velocity. Variables associated with the radar are antenna patterns, including location and magnitude of sidelobes in both sum and difference, antenna height above the earth's surface, data rate, and tracking filter bandwidth.

Appendix A contains the details of the computer programs used for the antenna and multipath computations, a dictionary of variable names, and simple program outline. These programs are not intended as final versions, no attempt was made to improve their efficiency.

2. Multipath Models

The basic earth and scattering models will be developed in this section. Only five of the many combinations will be considered:

a) Flat smooth earth, specular reflection

b) Spherical smooth earth, specular reflection

c) Spherical rough earth, specular reflection

d) Spherical rough earth, diffuse reflection

e) Spherical rough earth, composite reflections.

The flat earth model will be considered in detail because of its basic nature. Also, its solution will be used as part of the solution for the more complex cases.

a. Flat Smooth Earth, Specular Reflection

The problem of signal propagation between two points is illustrated below. Two terminals are shown at different heights above a flat, smooth ground plane characterized by a relative dielectric constant (ϵ_r). The point on the surface where the reflection occurs is a function of the terminal heights and the distance between. The problem is reciprocal, either terminal may be considered the transmission location.

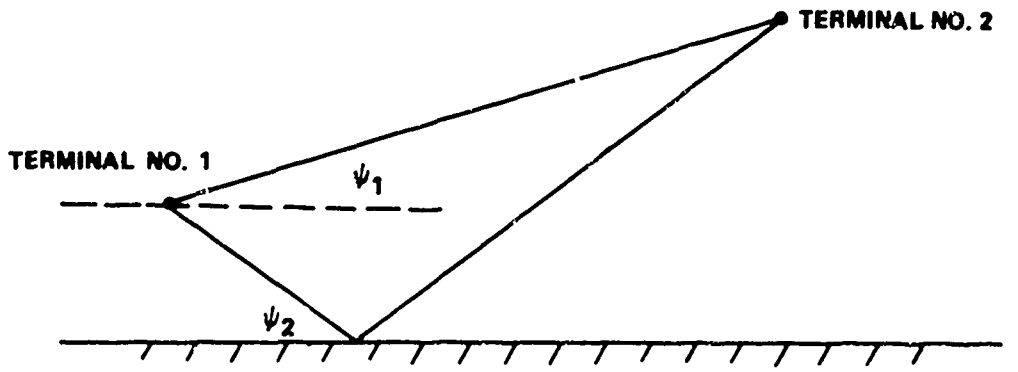

The justification for this rather simple geometrical optics model may be found in several texts, notably Beckmann and Spizzichino[1]. To a

[1] Beckmann, P., and Spizzichnio, A., The Scattering of Electromagnetic Waves from Rough Surfaces, MacMillan Co., New York, 1963.

first approximation, the reflection point may be considered as the center of the first Fresnel zone, i.e., the set of points on the surface with path length difference less than a half wavelength. Geometrical optics will be used throughout this report to determine the location of the reflection point.

The amplitude of the reflected energy is determined by the reflection coefficient at the earth's surface. For the case of vertical polarization of the transmitted and received signals, the reflection coefficient given by Kerr[2] is

$$\Gamma_v = \rho_v e^{-j\phi_v} = \frac{\left(\frac{K_1}{K_0}\right)^2 \sin\psi_2 - \sqrt{\left(\frac{K_1}{K_0}\right)^2 - \cos^2\psi_2}}{\left(\frac{K_1}{K_0}\right)^2 \sin\psi_2 + \sqrt{\left(\frac{K_1}{K_0}\right)^2 - \cos^2\psi_2}}$$

where

K_1 = electromagnetic propagation factor (complex)
K_0 = freespace propagation factor (complex)
ψ_2 = grazing angle
Γ_v = complex reflection coefficient
ρ_v = magnitude of reflection coefficient

and

$K = \sigma + j\omega\epsilon$
σ = conductivity of medium
ω = radian frequency of energy
ϵ = permittivity of medium.

[2] Kerr, D. E., Propagation of Short Radio Waves, McGraw-Hill Book Co., New York, 1951.

For most soil conditions under consideration $\epsilon >> \sigma$ so that $K = j\omega\epsilon$ and the above expression becomes

$$\rho_v = \frac{\epsilon_r \sin \psi_2 - \sqrt{\epsilon_r - \cos^2 \psi_2}}{\epsilon_r \sin \psi_2 + \sqrt{\epsilon_r - \cos^2 \psi_2}}$$

Therefore, the reflection coefficient is no longer a complex quantity and has no effect on the phase of the reflected signal. However, when ψ_2 becomes less than a critical angle, ψ_c (the complement of Brewster's polarizing angle), the reflected signal has a phase shift of π radians. Above this angle no phase shift occurs.

To illustrate how the signals must be combined a vector diagram will be useful. Assume that the direct path energy is taken as the reference. Its amplitude and phase depend, in general, upon such things as transmitted

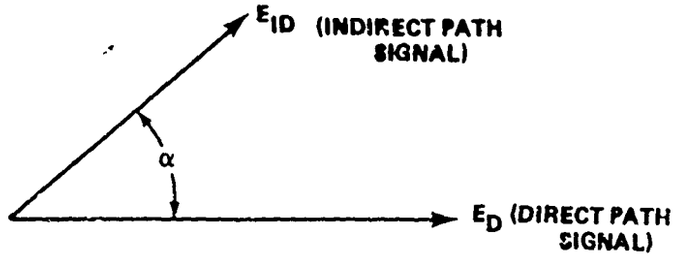

power, receiver antenna area, losses, and propagation path length and characteristics. For this discussion it may be taken as unity amplitude and zero phase angle. The indirect signal is scaled by the reflection coefficient magnitude and has a phase α determined by the path length difference and the possible π reflection phase. Then

$$\alpha = \frac{2\pi}{\lambda} \left(R_{ID} - R_D\right) \quad \text{for} \quad \psi_2 > \psi_c$$

and

$$\alpha = \frac{2\pi}{\lambda} \left(R_{ID} - R_D\right) + \pi \quad \text{for} \quad \psi_2 \leq \psi_c$$

where λ = wavelength.

This method of calculating α requires determination of R_D and R_{ID} quite accurately. This is well within the capability of the CDC 6600 computer used for this study, but problems have been encountered with other equipment. One method used to overcome this problem is to assume $\psi_2 \approx \psi_1$, thus allowing a simple calculation:

$$\alpha = \frac{2\pi}{\lambda} \left(2h_1 \sin \psi_1\right)$$

where h_1 is the height of terminal 1, and ψ_1 is the elevation angle of terminal 2 from terminal 1 (see sketch page 2).

b. Spherical Smooth Earth, Specular Reflection

The geometry of the spherical earth multipath problem with exaggerated dimensions is shown in the following sketch. In this model the geometrical optics reflection is with respect to the earth tangent at the point of reflection, so that in general the multipath points for a flat earth and a curved earth model are not the same. Several methods have been proposed for the calculation of the reflection location, and the best for use in this case was found in Kerr[3]. Once

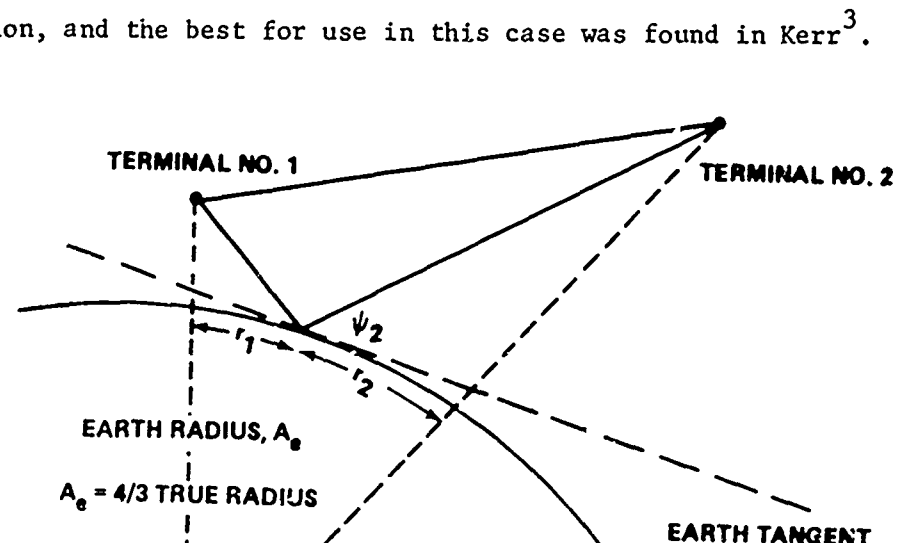

[3]Kerr, op. cit.

the geometrical problem is solved the reflection coefficient for vertical polarization may be calculated from

$$\rho_{sv} = \rho_v D$$

where ρ_v is the flat earth vertical polarization reflection coefficient, and D is the divergence factor caused by spherical reflection

$$D = \left(1 + \frac{4r_1 r_2}{A_e (r_1 + r_2) \sin 2\psi_2}\right)^{-\frac{1}{2}} .$$

All other parts of the calculation such as antenna scaling and phase calculations are handled exactly like the flat earth case. Derivations of the divergence factor D and the location of the reflection location are given in Kerr[4].

c. Spherical Rough Earth, Specular Reflection

When surface roughness is added to the model several new parameters become involved, and the character of the model changes. The models described so far have been deterministic in nature, but statistical methods must be used to describe the distribution of heights and spacings of the surface protrusions and of scattering from this surface.

In the case of a smooth surface all the indirect field is scattered specularly by the Fresnel zone described previously. As the surface is broken up by roughness this field decomposes into two components. One is the specular component, existing in the specular direction as defined by the smooth surface case. Its characteristics will be described in this paragraph. The other component is diffuse or noncoherent and exists in all directions; it will be described in the next paragraph.

If the surface is allowed to have varying vertical heights about the smooth surface as a mean, then the waves reflected from two adjacent points within the first Fresnel zone of height difference Δh will differ in phase by

$$\Delta\phi = \frac{4\pi\Delta h}{\lambda} \sin \psi_2 .$$

---

[4] Kerr, loc. cit.

Further, if it is assumed that the surface heights are normally distributed with standard deviation Δh and zero mean, then according to Beckmann[5] the distribution of the scattered energy consists of two components, a fixed component and a fluctuating component that is Hoyt distributed (orthogonal normal variates with zero means and unequal variances). The composite scattered field has a mean square value of

$$\overline{\rho_s^2} = e^{-(\Delta\phi)^2} \quad .$$

This is then used with the reflection coefficient of (b) to give the rough earth specular reflection coefficient

$$\rho_{rsv} = \rho_{sv}\, \rho_s D \quad .$$

For short transmission paths over land the coefficient may be taken as a constant given by the mean value expression. This was done in the study. Also, the adjacent surface features were assumed independent, and ρ_s calculated and used as indicated. However, other very important parameters are the correlation distance and the surface autocorrelation function. This surface correlation might be introduced in a manner similar to that used by Pope and Wood[6] to introduce correlation into simulated ground clutter data.

d. Spherical Rough Earth, Diffuse Reflection

The diffuse component of the rough earth scattering emanates from an area of the surface which is in general much larger than the first Fresnal zone. Beckmann[7] defines this area in terms of the terminal geometry and mean surface slope. Once this area is defined, calculation of the diffuse scattering coefficient, ρD, involves integration over the surface, the radar antenna pattern, and the target scattering characteristics. In order to simplify the model for this study, the

---

[5] Beckmann, loc. cit.

[6] Pope, B. E., and Wood, W. E., Digital Simulation of a Phase Monopulse Tracking Radar, U.S. Army Missile Command, Redstone Arsenal, Alabama, Report No. RE-TM-70-2, 28 January 1970 (Unclassified).

[7] Beckmann, loc. cit.

RMS diffuse scattering coefficient was defined as in the following diagram. This may be compared with the generalized results given by Beckmann[8] on page 340. The distribution was assumed Rayleigh, after Beckmann[9].

The point of origin of this scattering must also be determined. In most cases of interest in this study the diffuse return may be assumed to originate at the specular point. This may be invalid for elevation angles less than a few tenths of a degree. However, simulation runs with the diffuse scattering from other locations produced similar results. Therefore the specular and diffuse scattering components were assumed co-located in this study.

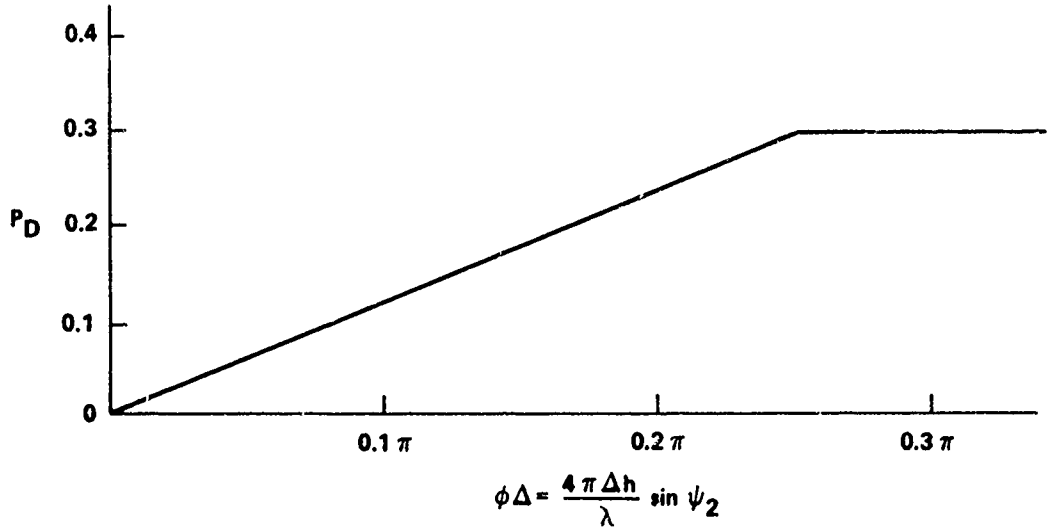

In this case the scattering coefficient becomes

$$\rho_{rsv} = \rho_{sv}\rho_D D$$

The divergence factor D may be removed from this expression according to Beckmann[10], because it has little effect on the diffuse scattered signal.

---

[8] Beckmann, loc. cit.

[9] Beckmann, Ibid.

[10] Beckmann, loc. cit.

e. Spherical Rough Earth, Combined Reflections

Rough surfaces may be taken as those which satisfy the Rayleigh criterion,

$$\Delta\phi < \frac{\pi}{2} \quad .$$

This may also be expressed in terms of the grazing angle and RMS surface height as

$$\sin \psi_2 < \frac{\lambda}{8\Delta h} \quad .$$

Thus, it can be seen that a surface may be rough in the Rayleigh sense in one grazing angle region and smooth in another. This could be used to define the angular regions of importance of various types of scattering.

The diffuse and specular models may be used together in a composite model. The same equations are used and the signals combined as indicated in the vector diagram below.

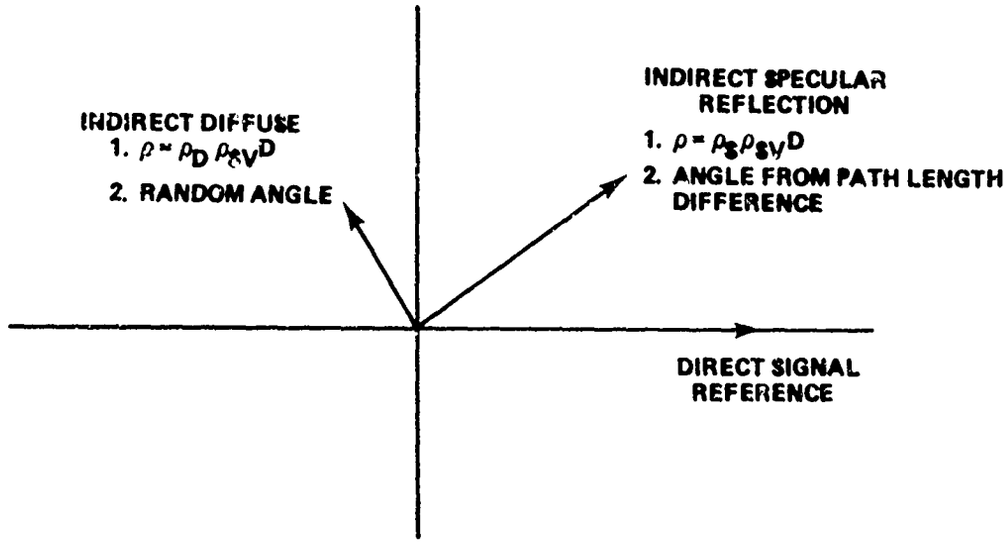

3. Radar and Target Models

a. Radar Model

The radar model used for this study is described below in block diagram form.

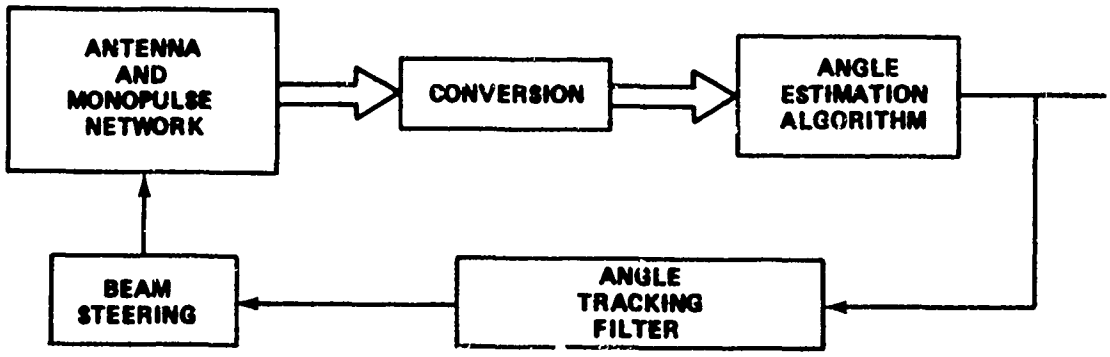

The basic antenna model (Antenna) is a rectangular array space fed by four horns. On receive, these horn signals are combined to form amplitude monopulse sum and two difference voltages. These three signals are split into in-phase and quadrature components by the down conversion/mixer which is assumed ideal, as was the monopulse network. The phase of this local oscillator is selected randomly over two π radians. After analog-to-digital (A/D) conversion an angle measurement is made by the following algorithm:

$$\text{Angle Measurement} = \frac{(S_I \times D_I) + (S_Q \times D_Q)}{(S_I \times S_I + S_Q \times S_Q)} \times \text{Slope}$$

where

S_I = Sum in-phase component

S_Q = Sum quadrature component

D_I = Difference in phase component

D_Q = Difference quadrature component

Slope = Monopulse slope factor to convert error voltage to angle.

This measured angle is then smoothed by a critically damped GH filter and a prediction made for the next beam position. The filter beta was maintained at 0.8 and a sampling rate of 10 samples per second was used unless otherwise stated.

b. Target Model

For simplicity a constant cross section target of 1 square meter was flown radially outward from the radar.

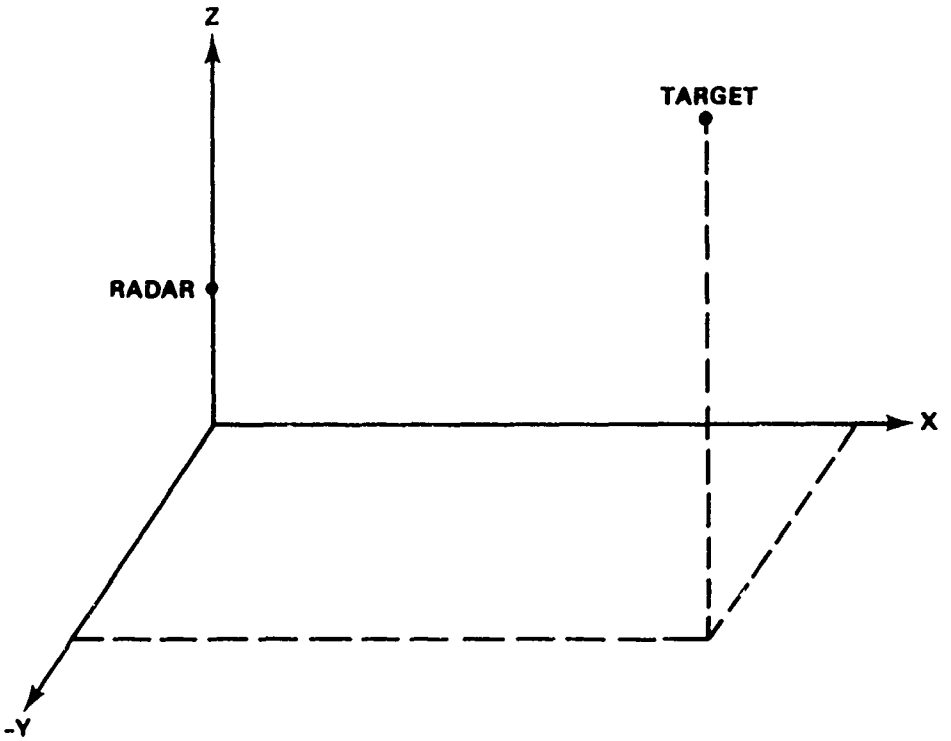

Initial values:

$$X_0 = 200 \text{ m}$$
$$Y_0 = 200 \text{ m}$$
$$Z_0 = 50 \text{ m}$$
$$\dot{X}_0 = 141 \text{ m/sec}$$
$$\dot{Y}_0 = 141 \text{ m/sec}$$
$$\dot{Z}_0 = 0 \quad .$$

4. Stability Requirements

During the investigation it was noted that some combinations of data rate, target velocity, and track filter bandwidth produced unstable angle tracking and in some cases complete loss of track.

Figure 1 shows a portion of the error profile where unstable operation was encountered but stable track recovered. The data rate-velocity-bandwidth space was mapped to locate the boundary between the stable and unstable regions for specular reflections only. The instability is observed as an oscillation as in Figure 1, and loss of track arbitrarily defined as an error in excess of 30 millisines. The space thus defined is shown in Figure 2, with the region of stable operation located below the pictured surface (high velocity and low sample rates are highly stable, low velocity and high data rate tend toward instability).

To explain this behavior, a stability analysis was undertaken. Since the combination of direct and indirect signals produced a time varying nonlinearity the analysis was done first for a no-multipath environment. This analysis is presented in Appendix B and outlined below.

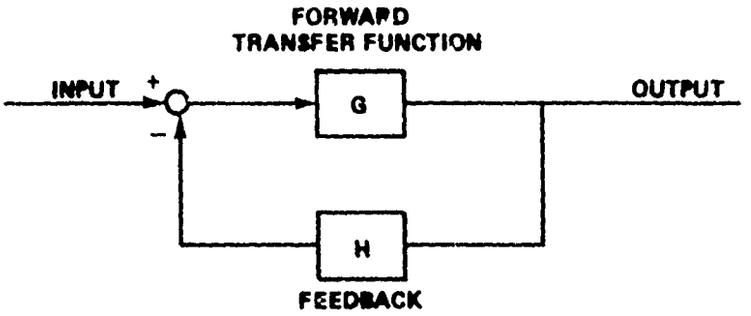

The forward transfer function may be considered as two separate blocks for clarity.

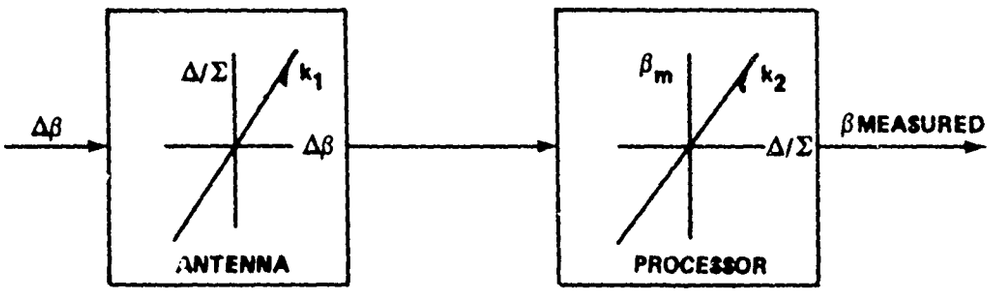

The previous sketch represents actual system parameters where:

$\frac{\Delta}{\Sigma}$ = Difference/sum voltage ratio

$\Delta\beta$ = Input angle error

β_m = Measured angle error

$$\frac{\Delta}{\Sigma} = k_1 \Delta\beta$$
$$\beta_m = k_2 \left(\frac{\Delta}{\Sigma}\right) \quad .$$

For Antenna 1 and matched conditions

$$k_1 \sim 82.5 \text{ volt/volt/radian}$$

$$k_2 \sim 0.01208 \text{ radian/volt/volt} \quad .$$

For the actual analysis of the system these two may be combined into one transfer block with gain K given by $k_1 k_2$. Note that for normal or "matched" operation K = 1. This transfer function is shown below:

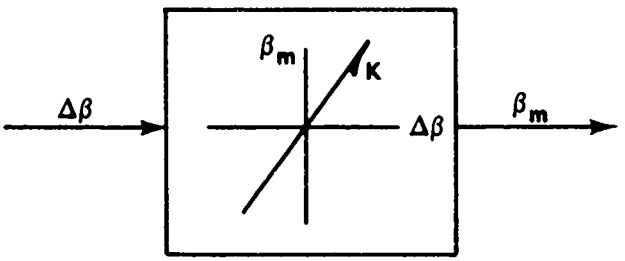

The analysis using the forward transfer function produced the following stability criteria as a funtion of beta, the bandwidth factor for the feedback path (see the following sketch).

The analysis proved that as long as the system transfer function is linear and matched values are used ($k_1 = 1/k_2$) the system is stable. However, the processor gain may be improperly chosen so that instability occurs.

A few comments on Δ/Σ curves are appropriate. As shown in Appendix B, these curves are nonlinear and in some cases may be linearized over only a limited region. Selection of a linear function for the inverse, k_2, is always somewhat in error. Therefore the idea of matched antenna and processor is only an ideal.

When multipath propagation is added to the problem, the forward transfer function becomes time-varying nonlinear. However, the remainder of the system is unchanged, so that the stability criteria derived for the no-multipath case still apply. Referring to Figure 11, the instability only occurs at the multipath peaks at 0.8 and 0.4 degree elevation angles. The limitation to the two locations may be explained by reference delta/sum (D/S) curves produced at these points.

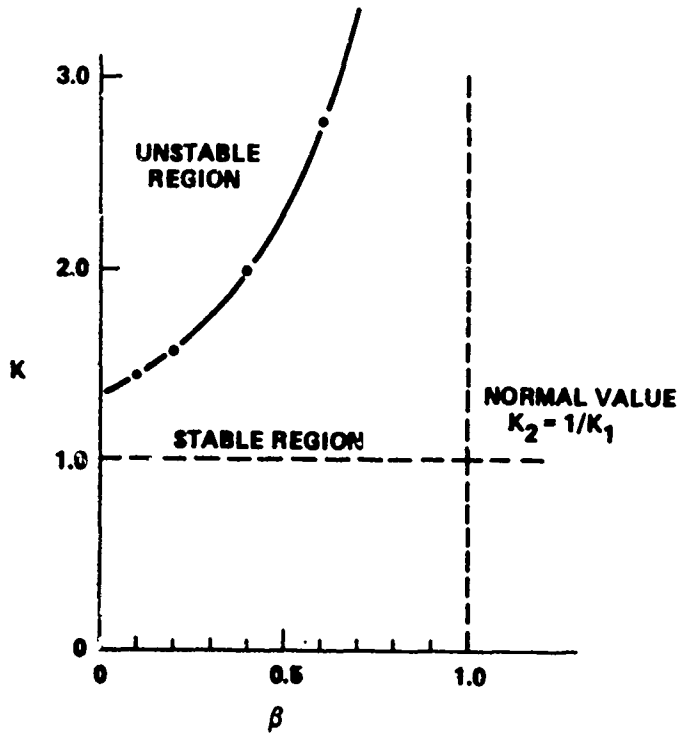

D/S curves and transfer functions were generated for the error peak located at 0.8-degree elevation to show how the slope stability criteria may be applied. The D/S curves are given in Figures 3, 4, 5, and 6. The first and last of these figures are for stable locations, while the other two are on the unstable peak. Each curve was generated by placing a stationary target at the elevation angle indicated, and the antenna swept to produce the D/S curve. These figures may be compared with Figure 11 to determine their relationship with error direction and magnitude.

Transfer functions of the form $\beta_m = K\Delta\beta$ were then developed from the D/S curves and $k_2 = 0.01208$ radian/volt/volt. These are shown in Figures 7, 8, 9, and 10 which correspond to the preceding D/S curves. Stability limits for selected values of beta from the stability analysis are shown in Figure 8.

The difference between complete loss of track as defined in this case and unstable track with recovery is a function of the data rate and target velocity. Stated qualitatively this reduces to the following: the more samples taken in the unstable region, the greater the effect on angle tracking. Therefore, low velocities and high data rates allow many measurements, while high velocities and lower data rates reduce the number of measurements taken while the system is prone to instability. (This agrees with the volume in Figure 2.) The amount that K exceeds the stability requirement also effects the number of samples needed for loss of track.

5. Results

Computer runs were organized to determine the sensitivity of multipath error to target altitude, target velocity, earth dielectric constant and roughness, antenna height and pattern, and the path length difference algorithm. For convenience the target was started close to the radar and flown radially outward. A few selected cases were run for incoming targets and the results were almost identical.

It was determined early in the effort that the only two geometrical variables of interest were the radar antenna height and the elevation angle of the target. Thus target altitude and range do not appear on the plots.

Figure 11 shows the low sensitivity of multipath errors to earth relative dielectric constant.

Figure 12 shows a similar but more pronounced effect when surface roughness is considered in a specular model. Larger values of RMS surface height tend to reduce the specular component, but increase the diffuse component as shown in Figure 13. Note that Figure 13 illustrates the envelope of the error, which appeared as a noise voltage. This was expected because the phase angle was drawn from a random uniform population. When both specular and diffuse scattering are present the result appears as a superposition of the incoherent diffuse component and the highly coherent specular component. The envelope of the errors are shown in Figure 14. It can be seen that the random diffuse errors are distributed about the specular error as a mean value.

A much larger variation in results occurred when changes in antenna height and pattern were allowed. Figures 15 and 16 illustrate the antennas used, the major difference being in the width of difference pattern major lobes and the location of nulls. Antenna 1 has coincident sum and difference nulls so that narrow difference lobes result. Antenna 2 has broad difference lobes. Both sum beams have a 3 dB beamwidth of 1.6 degrees in azimuth and elevation. The two antenna heights were chosen for comparison with other published results. Figures 17 and 18 show the type results encountered. Changing the antenna height relocates the maximum multipath errors in the region below 2 degrees. Not only are the locations changed, but the maximum values change. Changing the antenna model (Figure 18) also produced drastic changes. Note that this run is plotted on a different scale, because the errors were considerably larger than previous values. Several variants of both antennas were run at both heights with similar results: the location and magnitude of the peaks were in general unpredictable, but no errors above 18 to 20 millisines were observed.

The approximate algorithm for calculating path length difference mentioned in Paragraph 4 was also run for comparison. Figures 19 and 20

show the results. In the first case Antenna 1 was used at a 4 meter altitude, in the second case Antenna 2 was used at a 3 meter altitude. In general this algorithm produced results similar to the exact solution with slightly different peak magnitudes and locations.

In addition, some runs were made with the antenna constrained to operate only above certain elevation angle limits, sometimes called super-elevation tracking. The multipath errors were reduced in magnitude but not eliminated entirely.

6. Conclusions

This study has shown that multipath errors can be significant in a narrow beam tracking radar. These errors are almost independent of the relative earth dielectric constant. Surface roughness produces a more pronounced effect on both specular and diffuse returns. The location and magnitude of the major multipath errors are extremely sensitive to variations in antenna height and difference pattern structure, especially in the region of the peak lobe and first null. With the tracking filter in the loop most of the errors were below 10 millisines, and all were below 16 millisines. Some combinations of target velocity, angle tracking filter characteristics, and data rate produced unstable track situations.

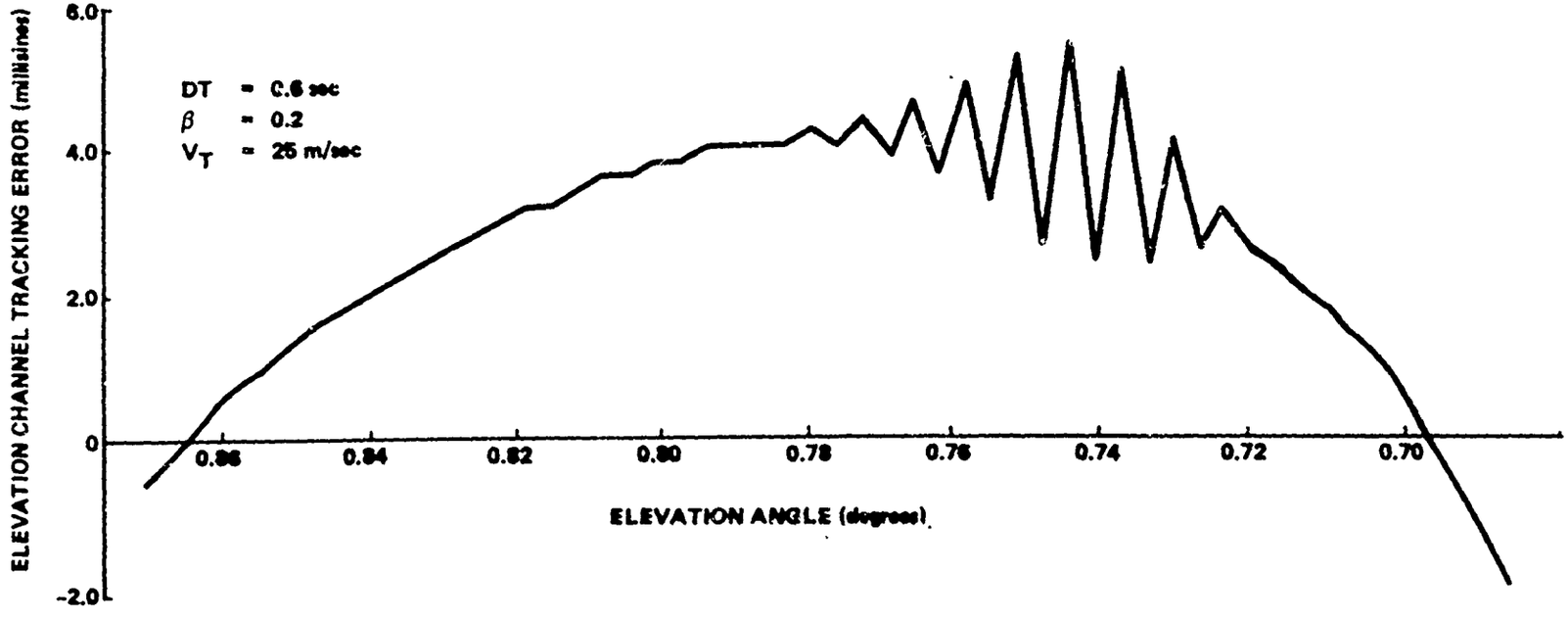

Figure 1. Unstable Tracking Region

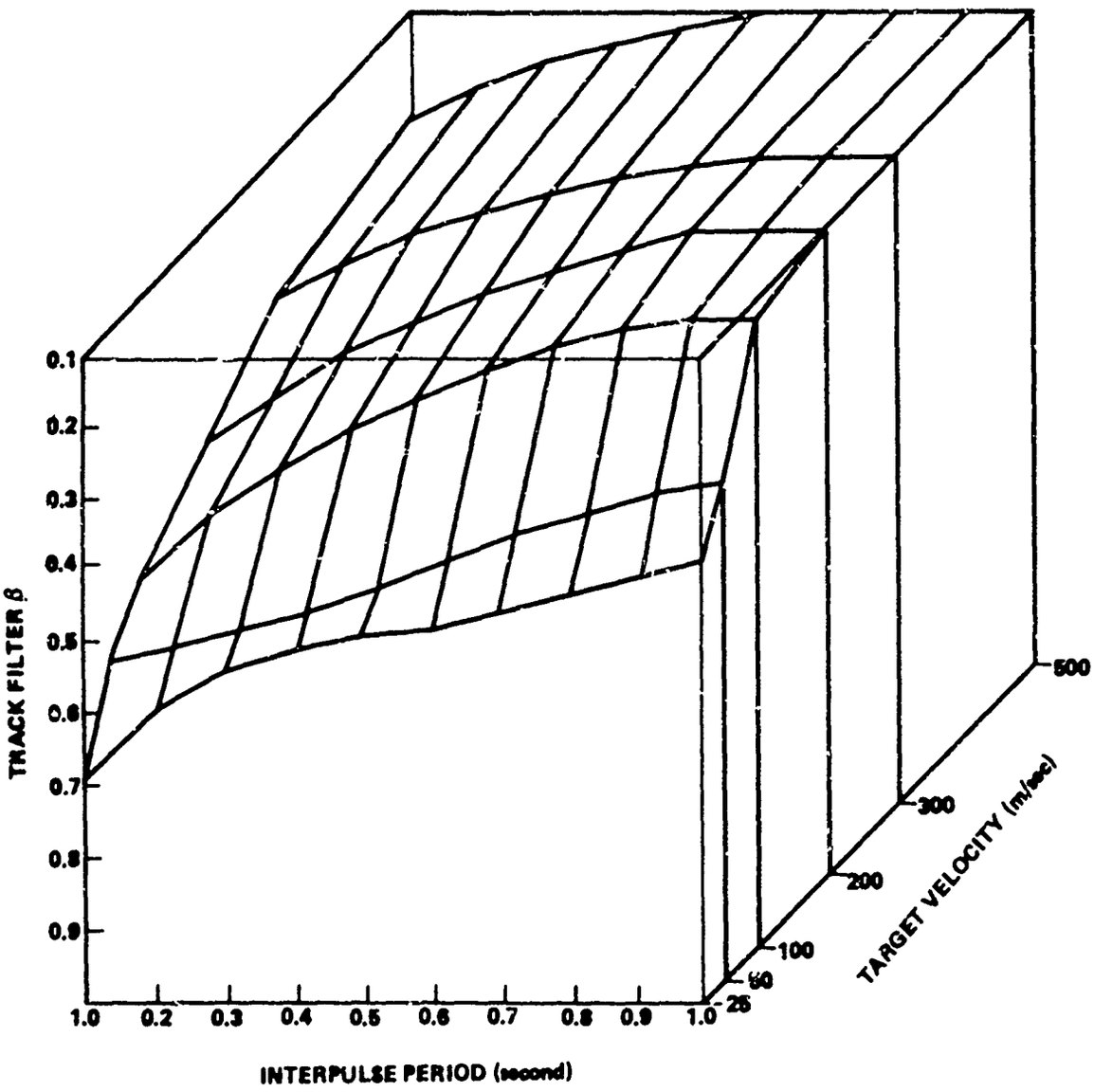

Figure 2. Tracking Volume

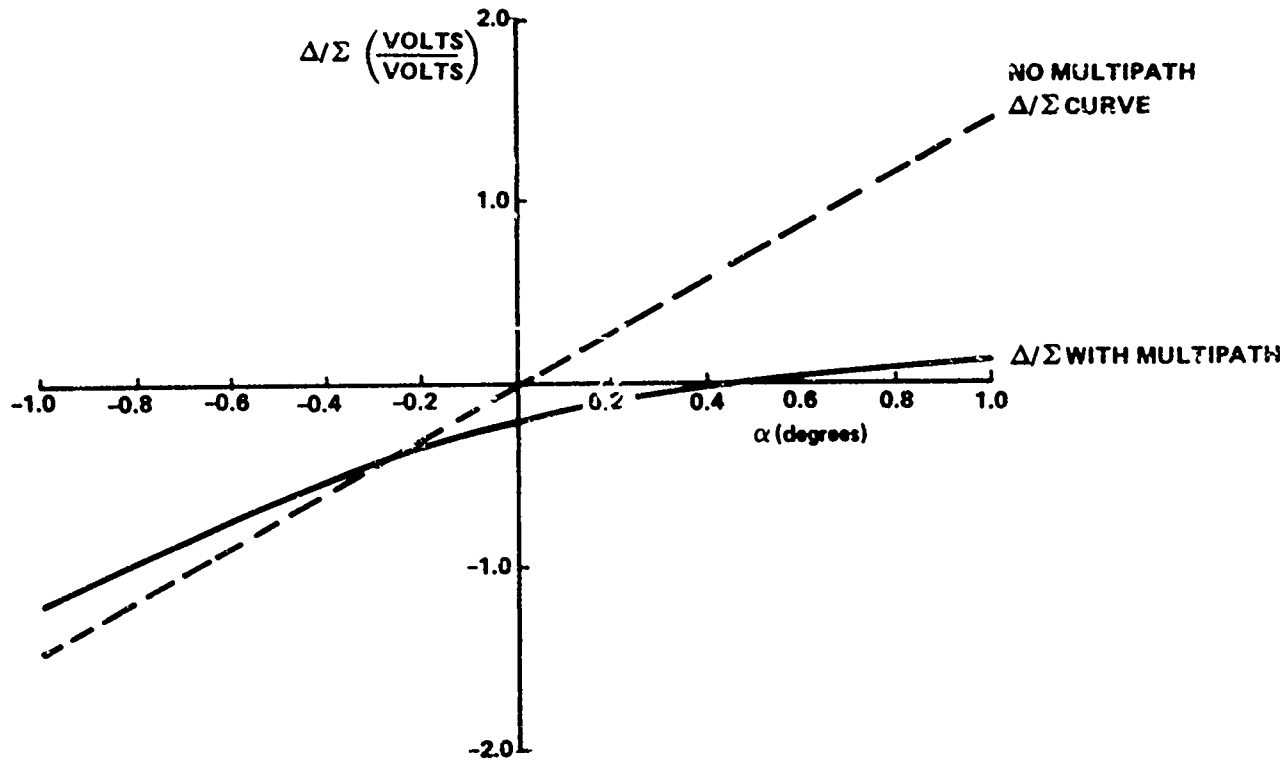

Figure 3. Δ/Σ Curve with Multipath, Elevation Angle = 0.94 Degree, Antenna 1

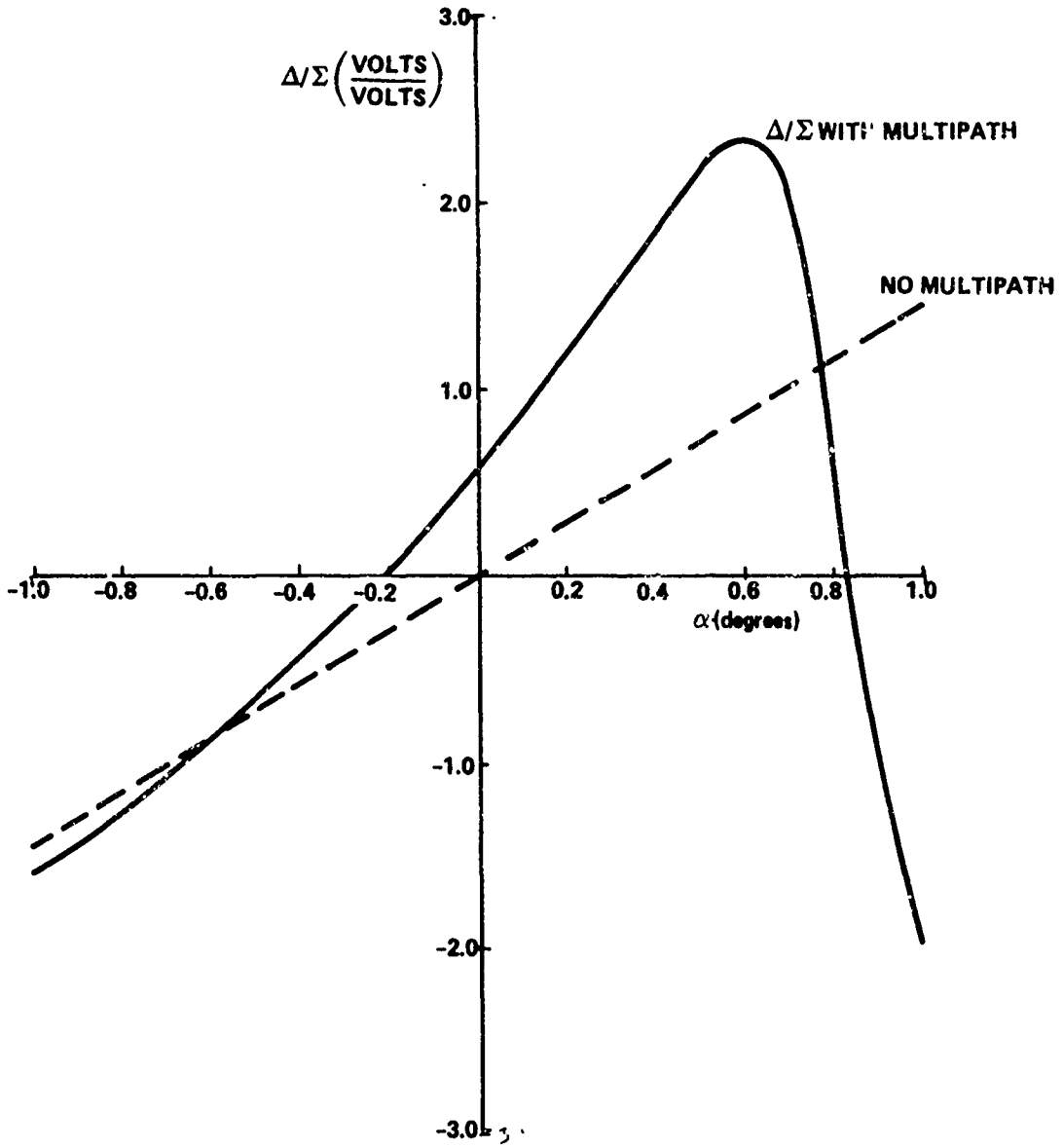

Figure 4. Δ/Σ Curve with Multipath, Elevation Angle = 0.81 Degree, Antenna 1

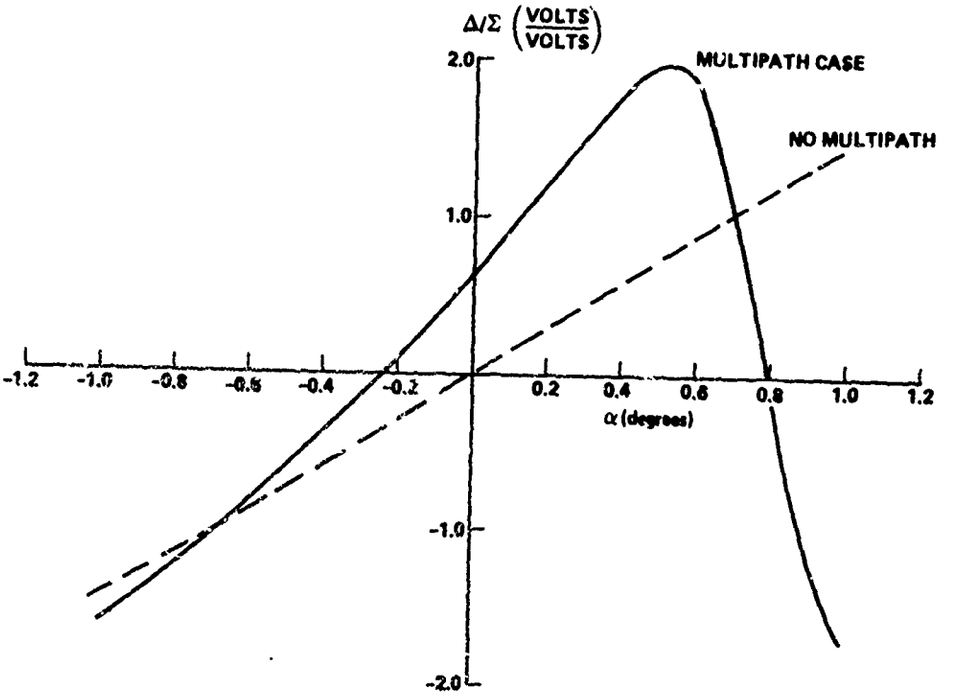

Figure 5. Δ/Σ Curve with Multipath, Elevation Angle = 0.75 Degree, Antenna 1

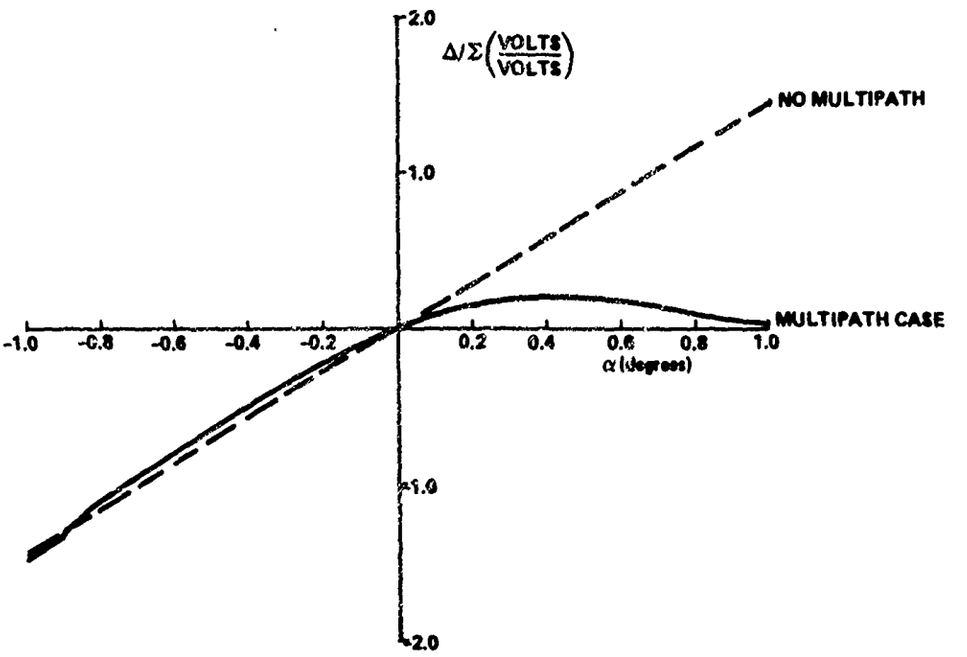

Figure 6. Δ/Σ Curve with Multipath, Elevation Angle = 0.70 Degree, Antenna 1

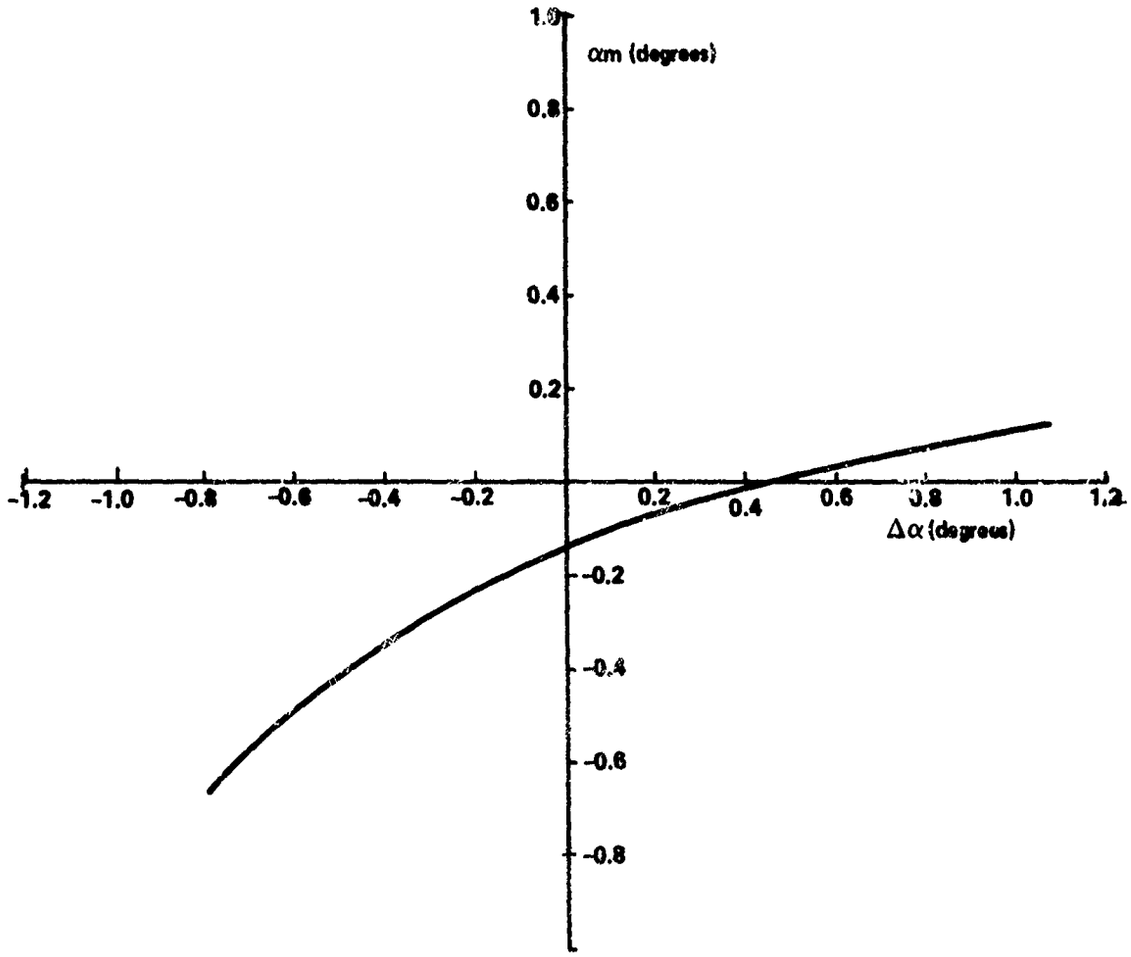

Figure 7. Radar Transfer Function, Elevation = 0.94 Degree, Antenna 1

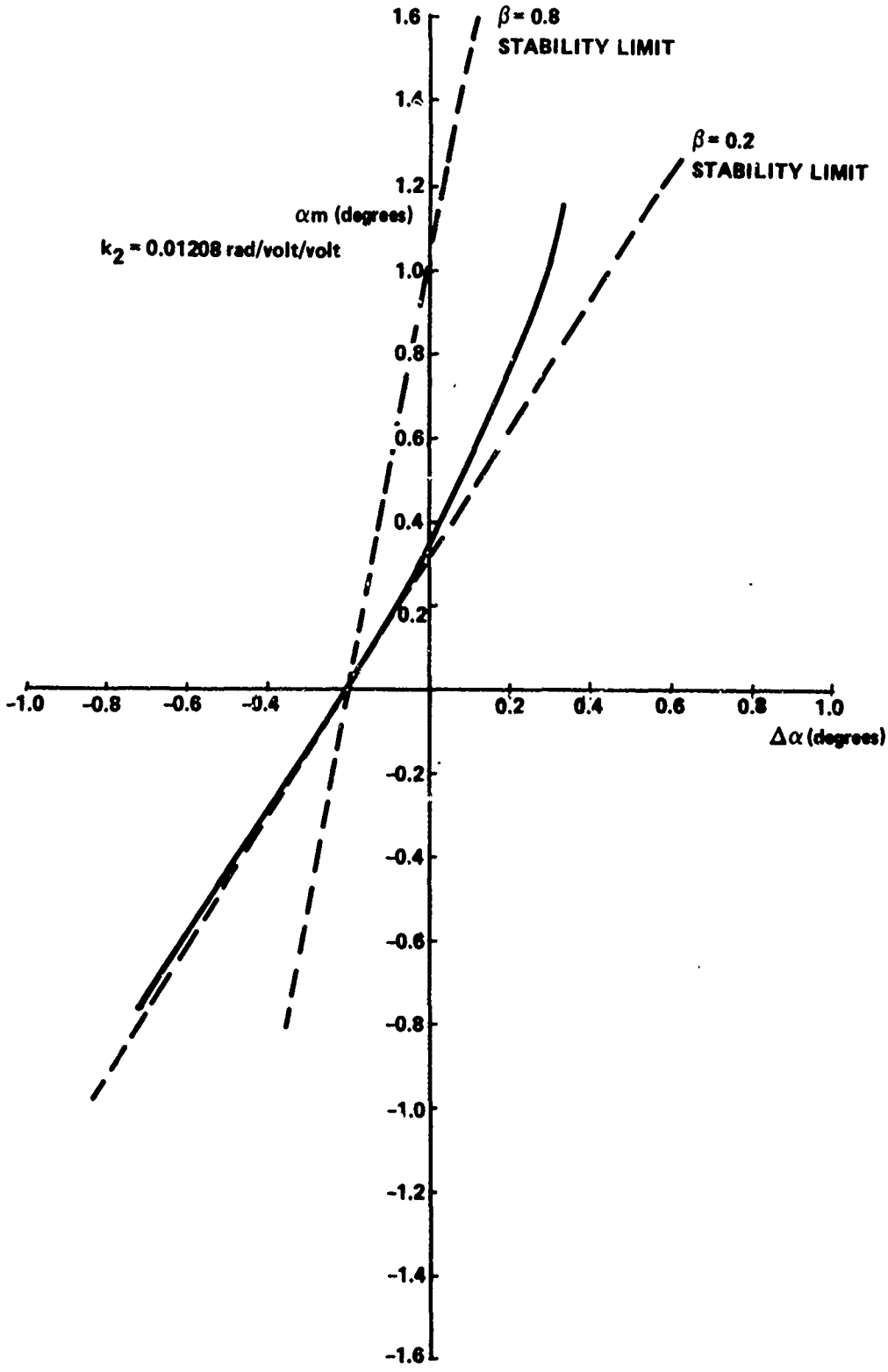

Figure 8. Radar Transfer Function, Elevation = 0.31 Degree, Antenna 1

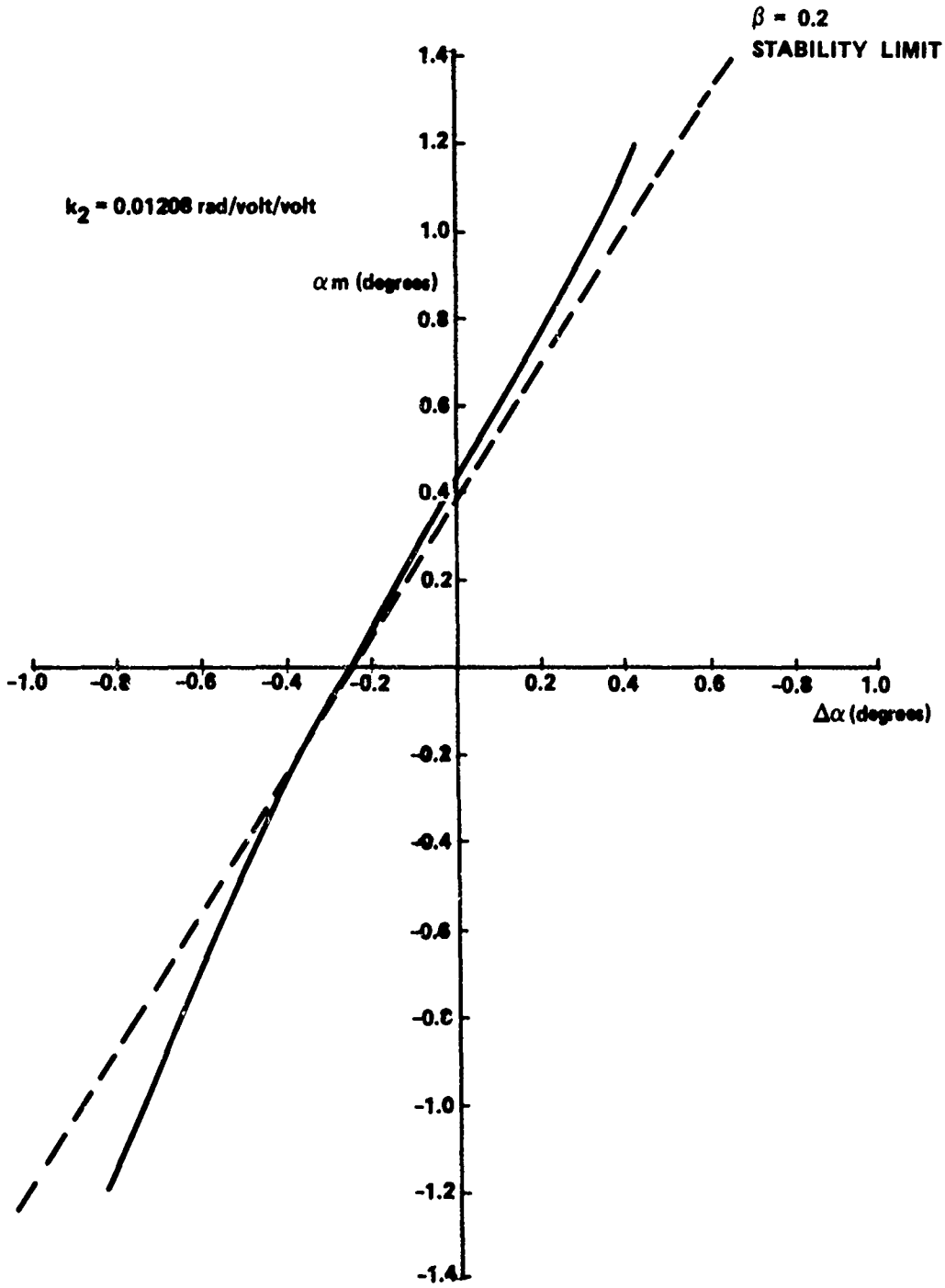

Figure 9. Radar Transfer Function, Elevation = 0.75 Degree, Antenna 1

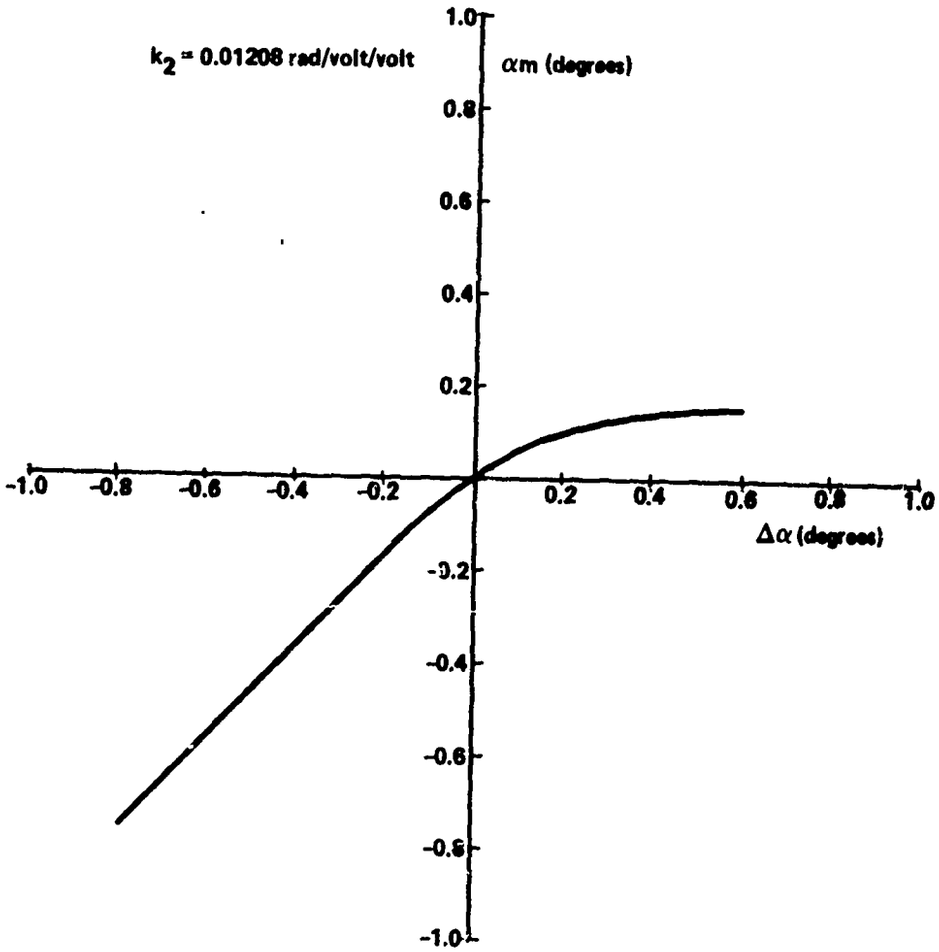

Figure 10. Radar Transfer Function, Elevation = 0.70 Degree, Antenna 1

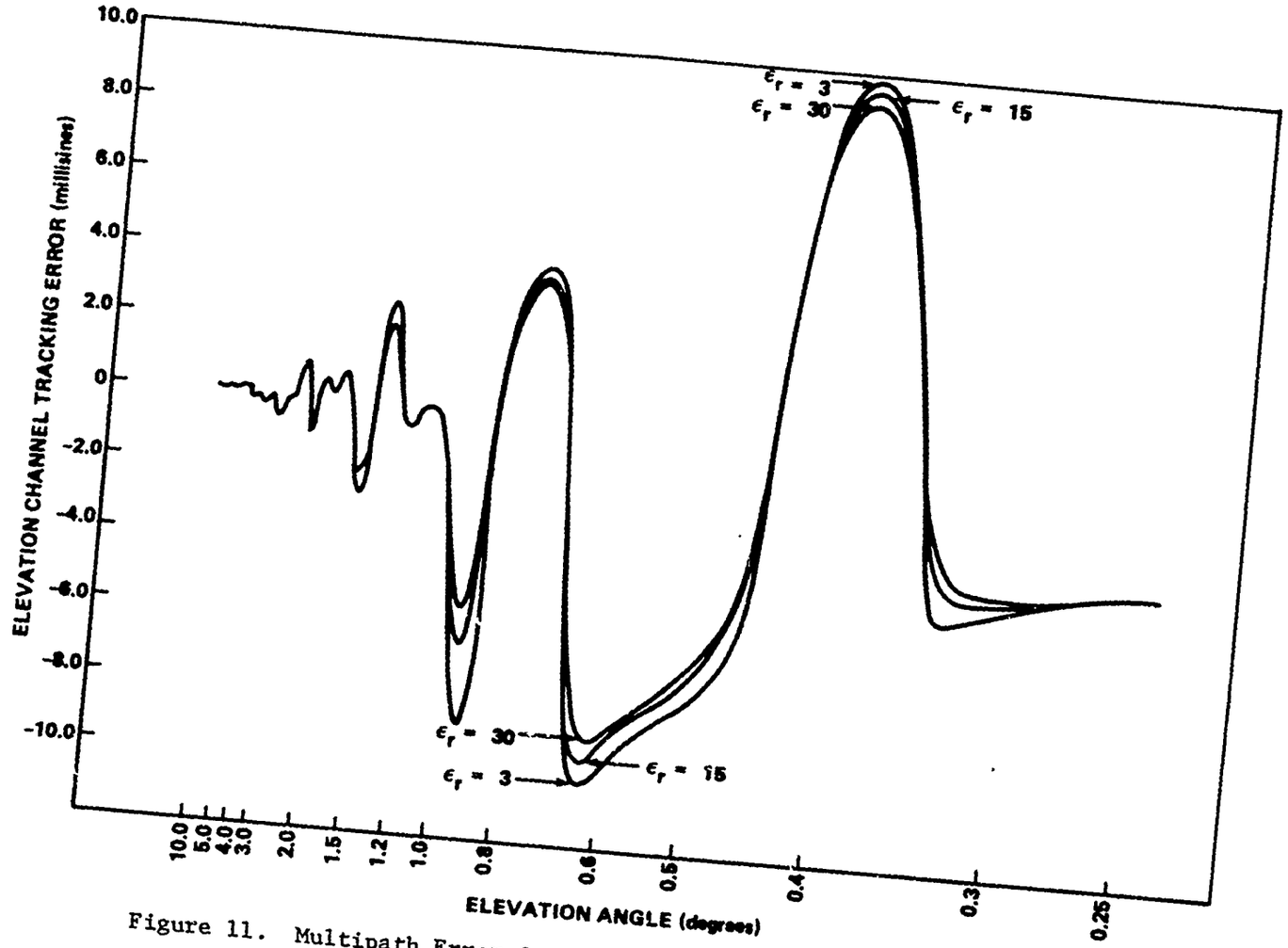

Figure 11. Multipath Error Specular Reflection Only, Smooth Earth

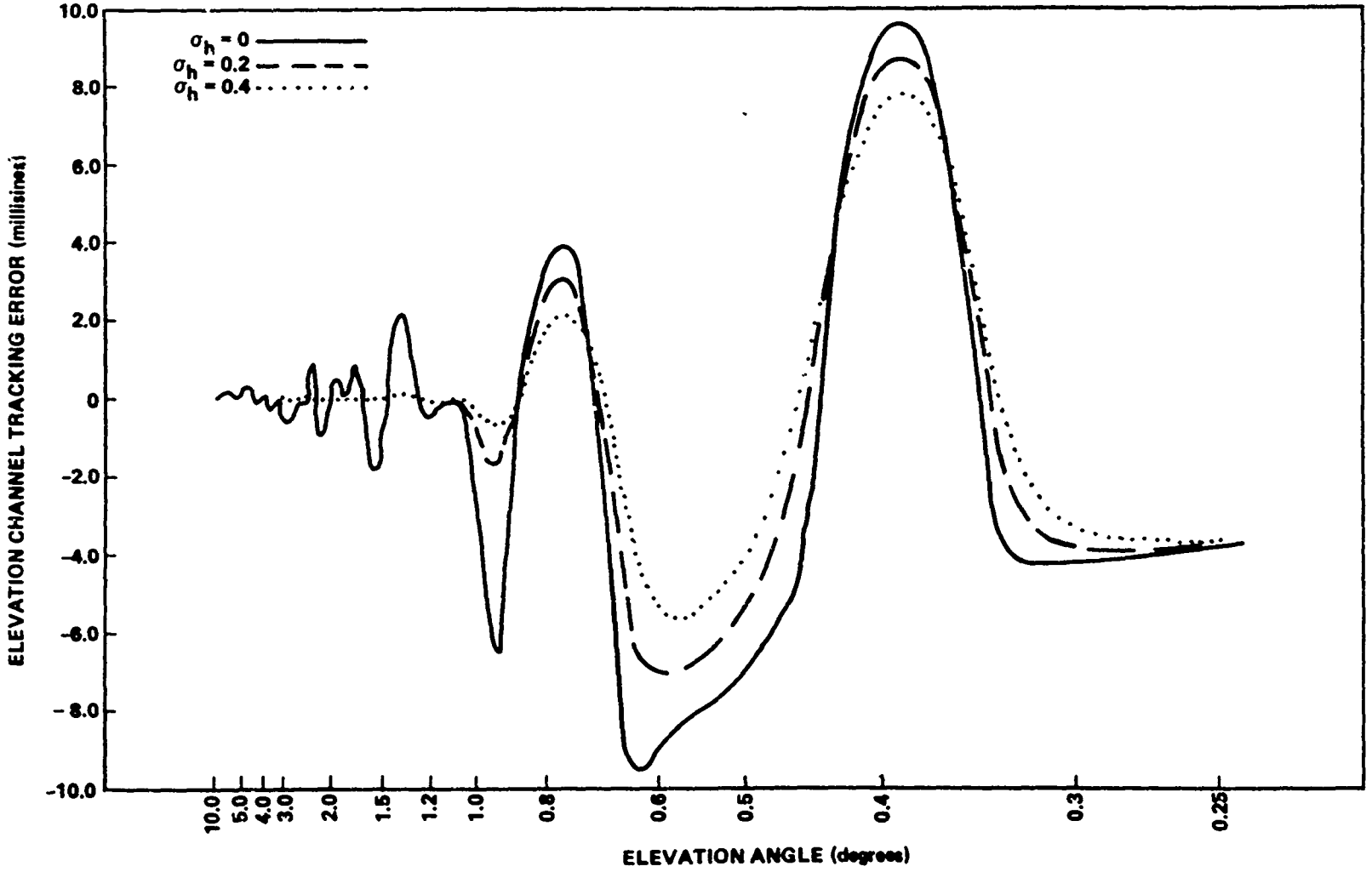

Figure 12. Multipath Error Specular Reflection from Rough Earth

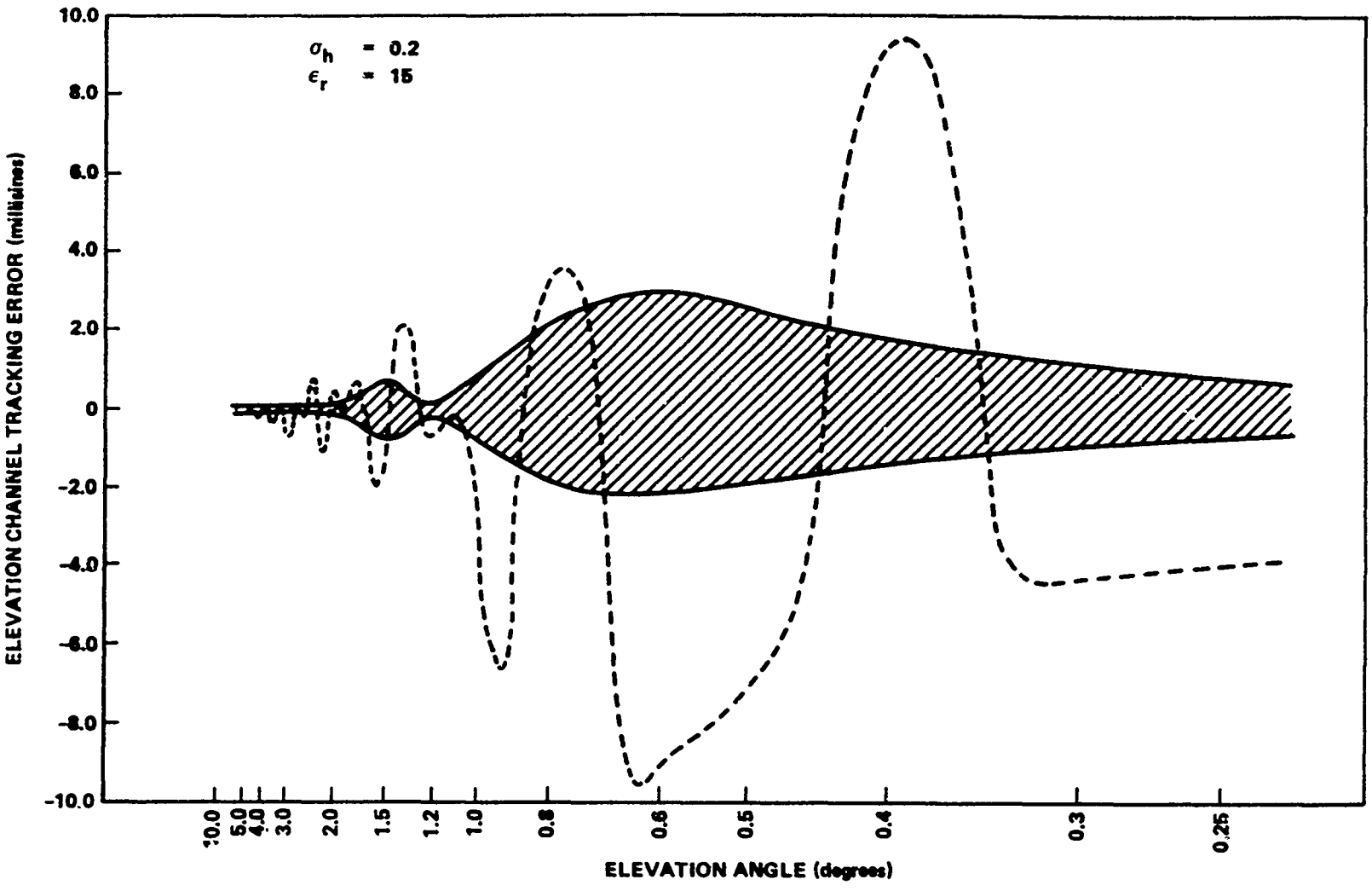

Figure 13. Multipath Error Diffuse Reflection, Rough Earth, Shaded (Specular Shown for Comparison)

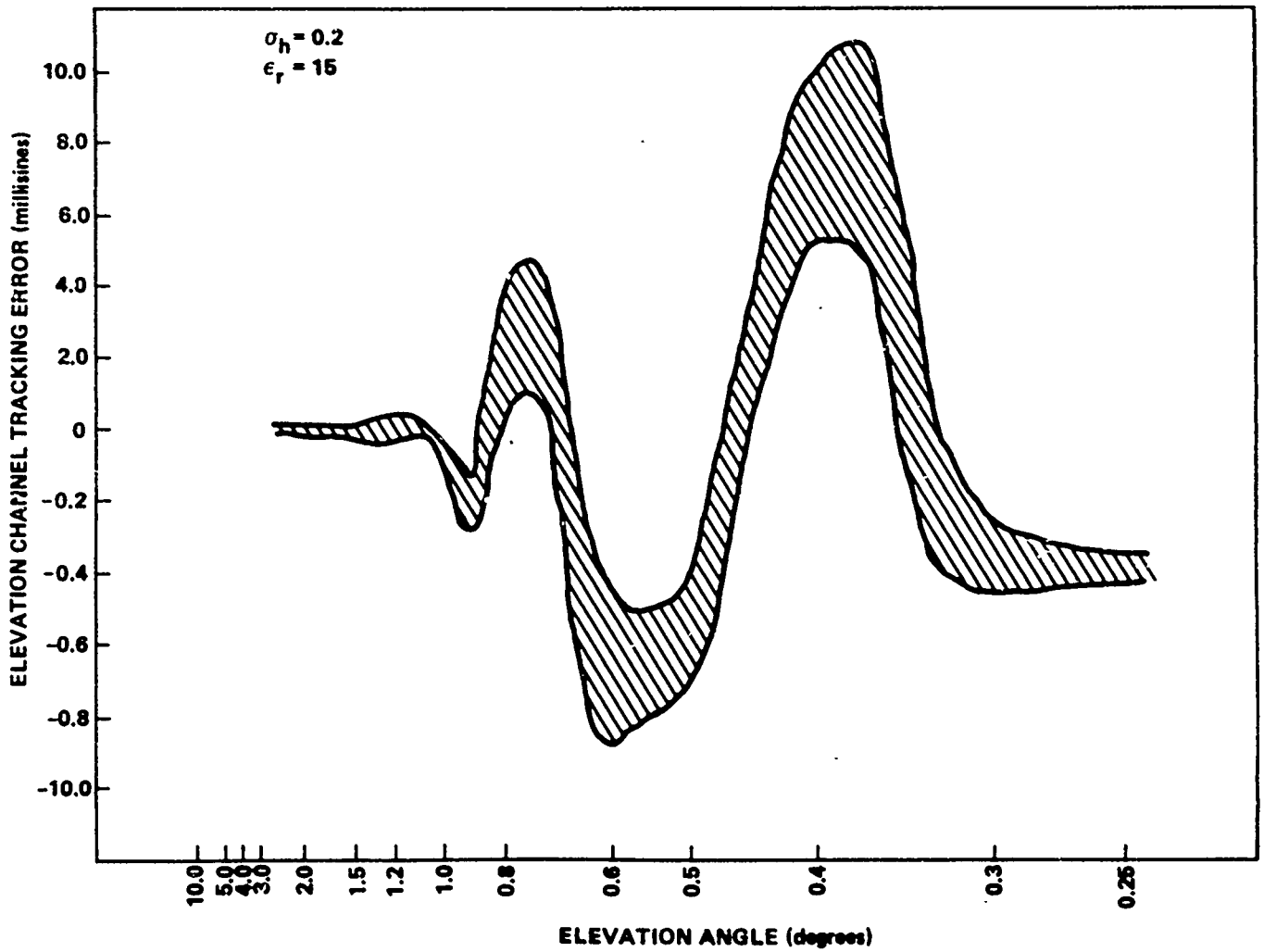

Figure 14. Multipath Tracking Error, Composite Model

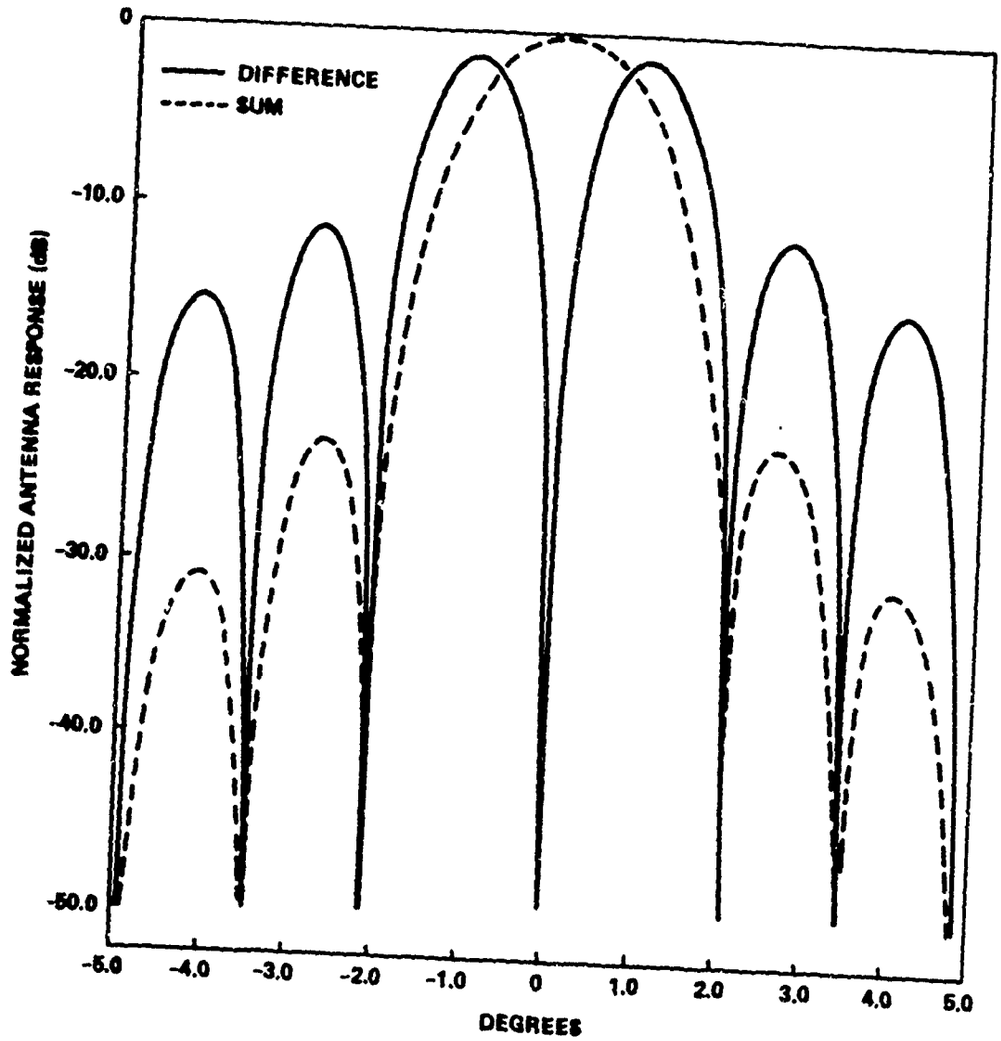

Figure 15. Antenna 1 Patterns

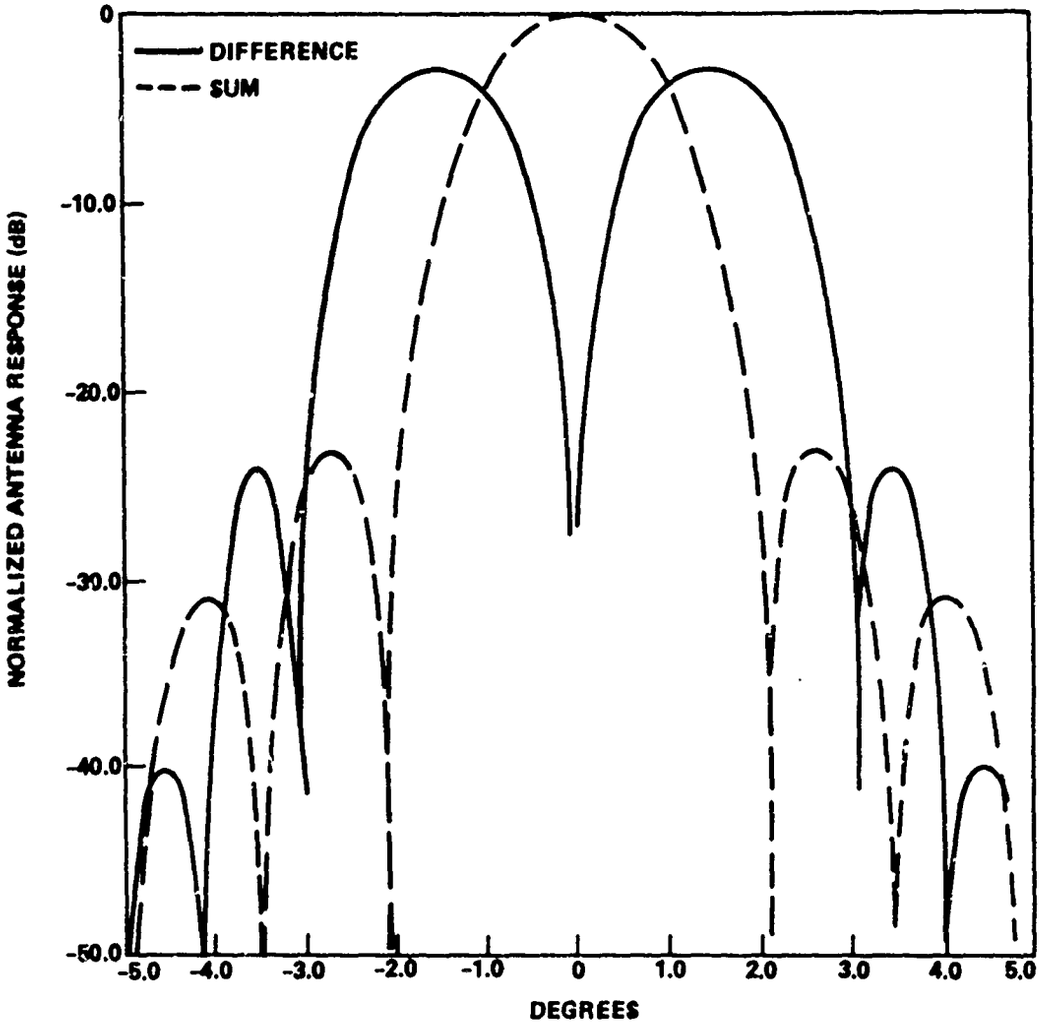

Figure 16. Antenna 2 Patterns

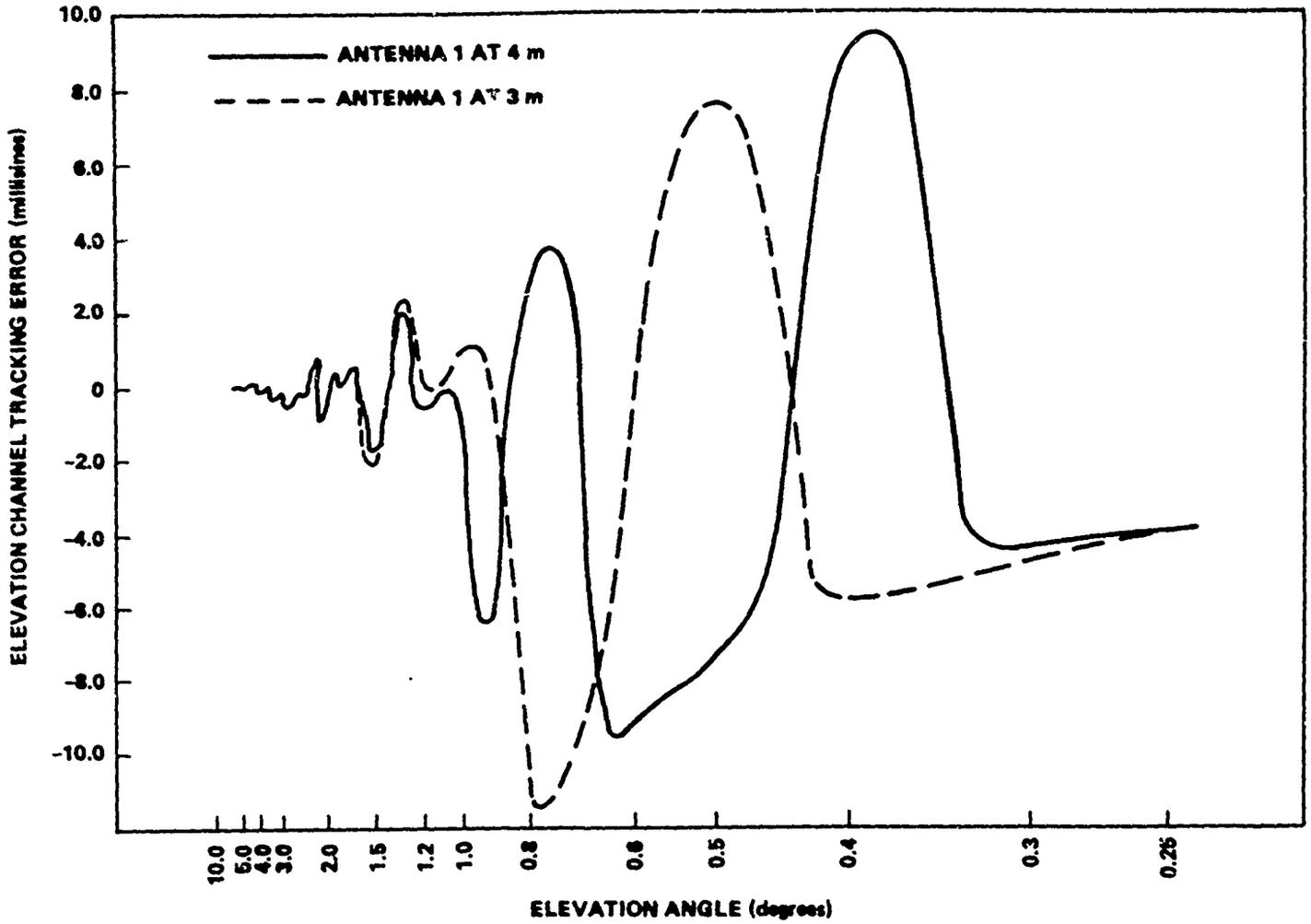

Figure 17. Multipath Tracking Error

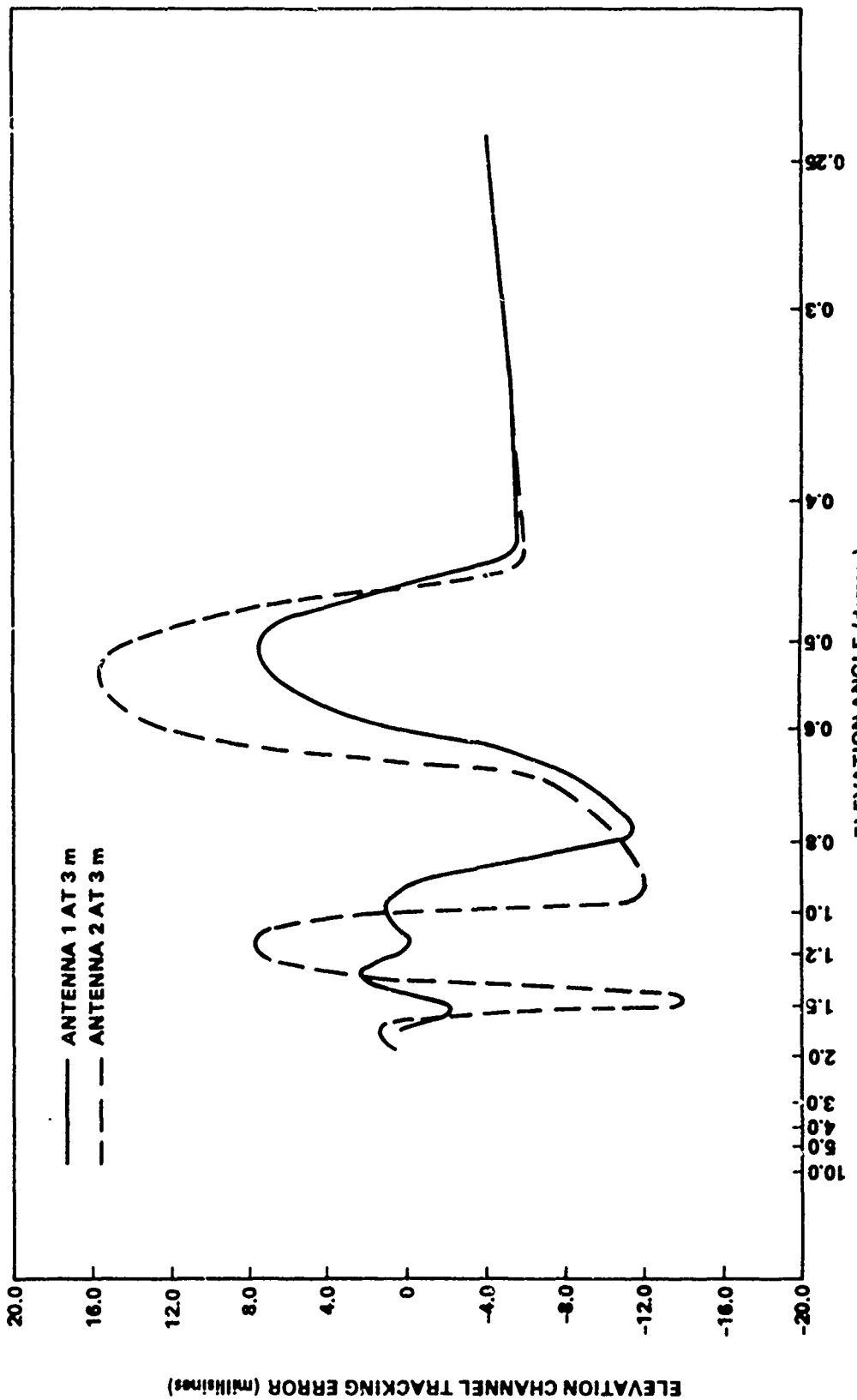

Figure 18. Multipath Tracking Error

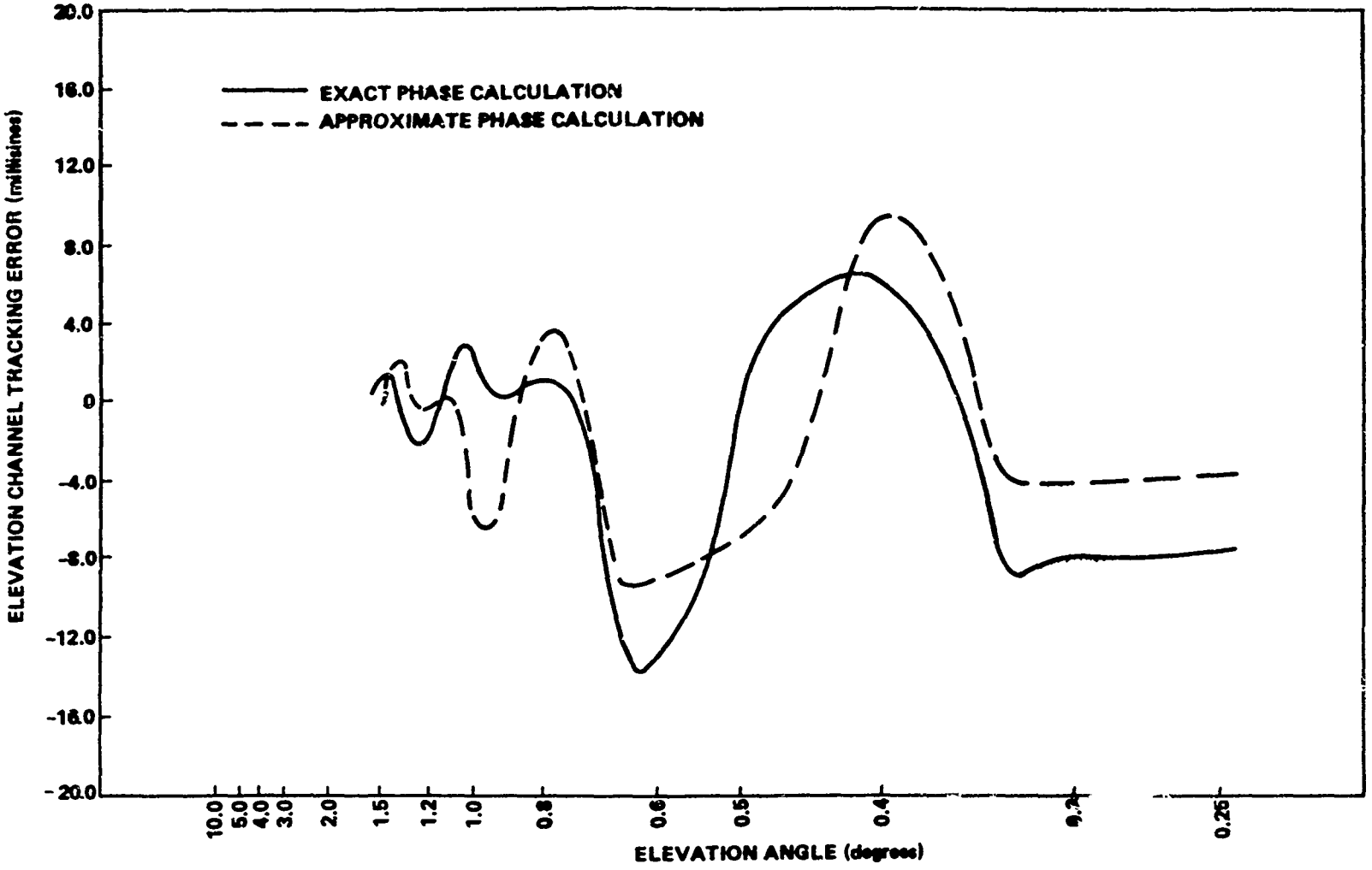

Figure 19. Multipath Tracking Error Specular Only, $\epsilon_r = 15, \sigma_h = 0$, Antenna 1 at 4 Meters

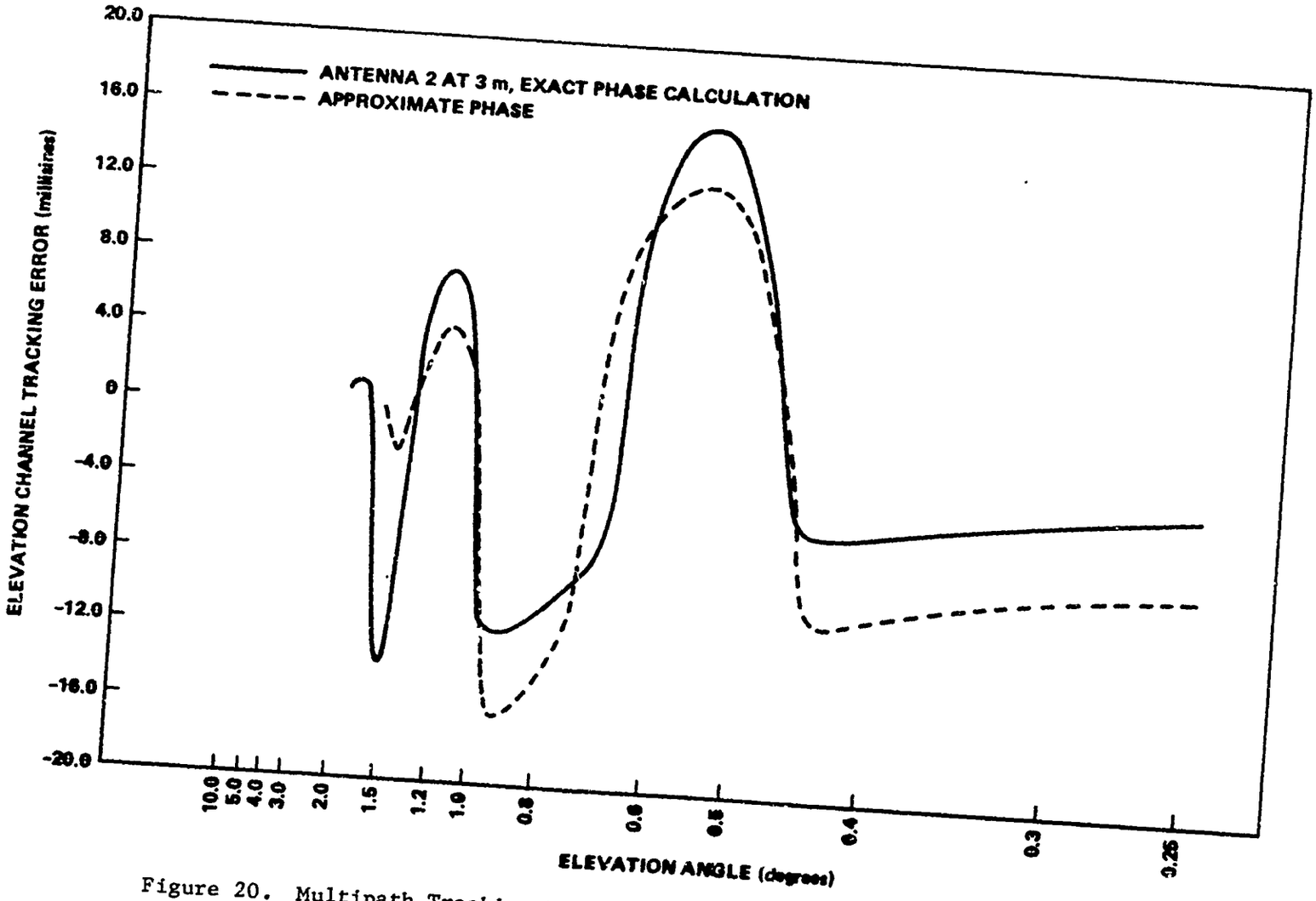

Figure 20. Multipath Tracking Error Specular Reflection, $\epsilon_r = 15$, $\sigma_h = 0$

Appendix A
PROGRAM LISTING AND DEFINITION OF VARIABLES

This appendix contains a listing of the multipath and antenna subroutines along with a variable list and comments.

The operation may be divided by line numbers as follows:

SUBROUTINE MULT

100 - 160	Dimension, complex and common statements
180 - 320	Determination of multipath point over spherical earth and conversion to radar coordinates
340 - 400	Determine phase relationship of direct and indirect signals
420 - 610	Determine reflection coefficient for specular and diffuse returns.
630	Calculate antenna response to direct signal
650	Calculate antenna response to indirect signals
770 - 820	Combine direct and indirect signals.

Dictionary of selected variables:

AE	Radius of 4/3 earth, 8.5 E + 06 meters
ALPM	Phase difference between direct and indirect signals
D	Spherical earth divergence factor
DFA	Complex antenna response in azimuth difference channel
DFE	Complex antenna response in elevation difference channel
DXR DYR DZR	Target velocities in array face rectangular coordinate
GAIN	Peak sum voltage gain
HA	Antenna height, meters
HT	Target Height, meters
PI	3.14159
PSIC	Critical reflection angle, radians
PS12	Grazing angle at multipath point, radians

R	Target range, meters
REFC	Flat earth vertical polarization reflection coefficient
REFCD	Diffuse reflection scattering factor
REFCS	Specular reflection scattering factor
SALP SBET	True target angles in radar sine space
SIGMH	RMS surface roughness height
SMUET SMULP	Multipath point angles in radar sine space
SUM	Complex antenna response in sum channel
SXALP SXBET	Predicted target position in radar sine space
WAVLN	Radar wavelength
XM YM ZM	Multipath point in rectangular coordinates
XN	Number of elements per row or column of array
ZN1	Real part complex relative earth dielectric constant

The listing of Subroutine MULT gives the exact method of calculating path length difference. To compare this with the approximate solution, lines 2770 through 2980 were changed or deleted to reflect the equations given at the end of Paragraph 2.a.

Subroutine ANTENA

930 - 960	Initial conditions
970 - 1100	Calculate antenna response

Dictionary of selected variables:

BW	Three dB sum beamwidth
DFA	Azimuth difference channel voltage
DFE	Elevation difference channel voltage
FO	Normalization factor
F1 F2 F3 F4	Responses at each of the four illumination horns

SALP SBET	Measurement angles in sine space
SNALP SNBET	Beam pointing angles in sine space
SUM	Sum channel voltage response
WAVLN	Wavelength of energy
XN	Number of elements in each row and column of the rectangular array

Two antenna models are referenced in this report. The listed version of Subroutine ANTENA calculates the response of Antenna Model 1. Antenna Model 2 was implemented by substitution of the following for line 1080:

```
X1 = SBET - SNBET

X2 = ABS (X1)

DX = X2 * 180.PI

IF (DX.GE.0..AND.DX.LE.3.) DE = 0.707 * SIN(180./3.*X1)

IF (DX.GT.3..AND.DX.LE.4.) DE = 0.063 * SIN [-180. * (X1-3. * PI/180.)]

IF (DX.GT.4.) DE = 0.01 * SIN [180. * (X1-4. * PI/180.)]

DFE = CMPLX (DE,0.)
```

```
      SUBROUTINE MULT(SNALP,SNBET,SALP,SBET,R,SUM,DFA,DFE,NN),RETURNS(M)MUL00100
      COMPLEX XIDD,XIDS,SUM,DFA,DFE,SUMD,DFAD,DFED                    MUL00110
      COMPLEX SUMID,DFAID,DFEID                                       MUL00120
      COMMON/MAIN/XR,YR,ZR,XT,YT,ZT,WAVLN,T,HA,DXR,DYR,DZR,XL         MUL00130
      NAMELIST/NAMMU/ZN1,SIGMH,XSPEC,XDIFF,GMA,BETAO                  MUL00140
      IF(R.LT.1.)GO TO 100                                            MUL00150
      DATA PI,C,AE/3.1415926536,2.997925E+08,8.5E+06/                 MUL00160
C                                                                     MUL00170
C DETERMINE LOCATION OF MULTIPATH POINT IN TARGET CO-ORDINATES        MUL00180
C                                                                     MUL00190
      Z=ZT+AE+HA          $HT=SQRT(XL**2+Z**2)-AE                     MUL00200
      S=AE*ACOS(Z/SQRT(XL**2+Z**2))                                   MUL00210
      P=2.*SQRT(AE/3.*(HT+HA)+((S/2.)**2)/3.)                         MUL00220
      PHI=ACOS(2.*AE*S*(HA-HT)/P**3)                                  MUL00230
      R1=S/2.+P*COS((PHI+PI)/3.)  $R2=S-R1                            MUL00240
      ZL=AE*COS(R1/AE)  $XLM=SQRT(AE**2-ZL**2)                        MUL00250
      ZM=ZL-AE-HA                                                     MUL00260
      XM=XLM*COS(ATAN2(YT,XT))            $YM=XLM*SIN(ATAN2(YT,XT))   MUL00270
      IF((AE**2)/ZL.GE.(AE+HA)) RETURN M                              MUL00280
C                                                                     MUL00290
C CONVERT TO RADAR CO-ORDINATES                                       MUL00300
C                                                                     MUL00310
      CALL CNVRT(XM,YM,ZM,A,B,D,SMULP,SMUET,GMA)                      MUL00320
C                                                                     MUL00330
C DETERMINE PATH LENGTH DIFFERENCE AND CRITICAL ANGLE                 MUL00340
C                                                                     MUL00350
      RID=SQRT(XM**2+YM**2+ZM**2)+SQRT((XT-XM)**2+(YT-YM)**2+(ZT-ZM)**2)MUL00360
      ALPM=2.*PI*(RID-R)/WAVLN                                        MUL00370
      PSI2=ATAN(XM/ZL)+ACOS((ABS(XM-XT))/SQRT((XM-XT)**2+(ZM-ZT)**2))MUL00380
      PSIC= ASIN(SQRT(1./(ZN1+1.)))                                   MUL00390
      IF(PSI2.LE.PSIC)ALPM=ALPM+PI                                    MUL00400
C                                                                     MUL00410
C CALCULATE REFLECTION COEFF AT MULTIPATH POINT                       MUL00420
C                                                                     MUL00430
      TERM1=ZN1*SIN(PSI2)                                             MUL00440
      TERM2=SQRT(ZN1-(COS(PSI2)**2))                                  MUL00450
      REFC=ABS((TERM1-TERM2)/(TERM1+TERM2))                           MUL00460
      D=1./SQRT(1.+4.*R1*R2/(AE*S*SIN(2.*PSI2)))                      MUL00470
      DELPHI=4.*SIGMH*SIN(PSI2)/WAVLN                                 MUL00480
      REFCS=SQRT(EXP(-(DELPHI*PI)**2))                                MUL00490
C                                                                     MUL00500
C PICK RAYLEIGH DISTRIBUTED SAMPLE                                    MUL00510
C                                                                     MUL00520
      SIGMD=0.35/0.25*DELPHI                                          MUL00530
      IF(DELPHI.GT.0.25)SIGMD=0.35                                    MUL00540
      SIGMD=SIGMD/SQRT(2.)                                            MUL00550
      CALL NORMAL(SIGMD,0.,V1)                                        MUL00560
      CALL NORMAL(SIGMD,0.,V2)                                        MUL00570
      REFCD=SQRT(V1**2+V2**2)                                         MUL00580
      ALPMD=RANF(U)*2.*PI                                             MUL00590
      XIDS=REFC*D*REFCS*CMPLX(COS(ALPM),SIN(ALPM))                    MUL00600
      XIDD=REFCD*REFC*CMPLX(COS(ALPMD),SIN(ALPMD))                    MUL00610
C                                                                     MUL00620
C CALCULATE DIRECT PATH ANTENNA GAIN                                  MUL00630
C                                                                     MUL00640
```

```
      CALL ANTENA(SNALP,SNBET,SALP,SBET,SUM,DFA,DFE,WAVLN,NN)          MUL00650
      SUMD=SUM                                                         MUL00660
      DFAD=DFA                                                         MUL00670
      DFED=DFE                                                         MUL00680
C                                                                      MUL00690
C CALCULATE INDIRECT PATH ANTENNA GAIN                                 MUL00700
C                                                                      MUL00710
      CALL ANTENA(SMULP,SMUET,SALP,SBET,SUM,DFA,DFE,WAVLN,NN)          MUL00720
      SUMID=SUM                                                        MUL00730
      DFEID=DFE                                                        MUL00740
      DFAID=DFA                                                        MUL00750
C                                                                      MUL00760
C COMBINE DIRECT AND INDIRECT SIGNALS                                  MUL00770
C                                                                      MUL00780
      SUM=SUMD+XSPEC*SUMID*XIDS+XDIFF*SUMID*XIDD                       MUL00790
      DFA=DFAD+XSPEC*DFAID*XIDS+XDIFF*DFAID*XIDD                       MUL00800
      DFE=DFED+XSPEC*DFEID*XIDS+XDIFF*DFEID*XIDD                       MUL00810
      RETURN                                                           MUL00820
  100 READ(5,NAMMU)                                                    MUL00830
      WRITE(6,NAMMU)                                                   MUL00840
      RETURN                                                           MUL00850
      END                                                              MUL00860


      SUBROUTINE ANTENA(SNALP,SNBET,SALP,SBET,SUM,DFA,DFE,WAVLN,NN)    MUL00870
C                                                                      MUL00880
C THIS SUBROUTINE DETERMINES THE RESPONSE IN FREE SPACE OF SINX/X PAT  MUL00890
C SNALP AND SNBET ARE THE BORESIGHT ANGLES IN SINES                    MUL00900
C SALP AND SBET ARE THE MEASUREMENT POINTS                             MUL00910
C                                                                      MUL00920
      COMPLEX UAHE, UBHE,UAHA,UBHA,SUM,DFA,DFE                         MUL00930
      NAMELIST/NAMAN/UAHA,UAHE,UBHE,UBHA,S                             MUL00940
      IF(NN.EQ.0)GO TO 100                                             MUL00950
      DATA PI,C,AE/3.1415926536,2.997925E+08,8.5E+06/                  MUL00960
      XN=NN                                                            MUL00970
      P1=PI*S*XN*1./WAVLN                                              MUL00980
      P2=P1/XN                                                         MUL00990
      P3=WAVLN/(2.*XN*S)                                               MUL01000
      F0=1./XN                                                         MUL01010
      F1=SIN(P1*(SNALP-SALP+P3))/SIN(P2*(SNALP-SALP+P3))*F0            MUL01020
      F2=SIN(P1*(SNALP-SALP-P3))/SIN(P2*(SNALP-SALP-P3))*F0            MUL01030
      F3=SIN(P1*(SNBET-SBET+P3))/SIN(P2*(SNBET-SBET+P3))*F0            MUL01040
      F4=SIN(P1*(SNBET-SBET-P3))/SIN(P2*(SNBET-SBET-P3))*F0            MUL01050
      SUM=CMPLX(.5*(F1+F2)*(F3+F4)/0.81069946,0.)                      MUL01060
      DFA=(F2-UBHA*F1)*(F3+F4)/(.81069946)*0.5                         MUL01070
      DFE=(F4-UBHE*F3)*(F1+F2)/     (0.81069946)*.5                    MUL01080
      DFA=UAHA*DFA                                                     MUL01090
      DFE=UAHE*DFE                                                     MUL01100
      RETURN                                                           MUL01110
  100 READ(5,NAMAN)                                                    MUL01120
      WRITE(6,NAMAN)                                                   MUL01130
      RETURN                                                           MUL01140
      END                                                              MUL01150
```

Appendix B
LINEAR STABILITY ANALYSIS

The angle tracking loop of this radar model may be analyzed as below.

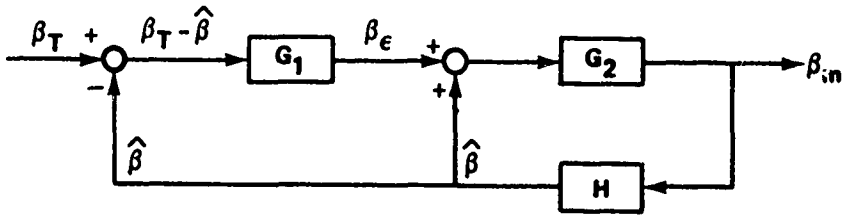

where

G = forward transfer function describing the radar angle measurement equations

H = feedback loop gain, here a critically damped gh filter.

β_T = true target position (SNBET)

$\hat{\beta}$ = predicted target position for next measurement (SHBET)

β_m = measured angle (SMBET)

β_ϵ = measured monopulse error signal (VM).

The names enclosed in parenthesis refer to varable names in the computer program listed in Appendix A. Following the computer listing, the forward block may be modeled as $\beta_\epsilon = K\ (\beta_T - \hat{\beta})$, or in sampled data transfer function notation $G_1(z) = K$. Thus the forward loop is considered as an impulse of weight K occurring at time n. Similarly $G_2(z) = 1$. The transfer function of the feedback loop may be derived from the three basic gh filter equations:

$$\bar{X}_n = \hat{X}_n + g\left(X_n - \hat{X}_n\right)$$

$$\bar{\dot{X}}_n = \bar{\dot{X}}_{n-1} + \frac{h}{T}\left(X_n - \hat{X}_n\right)$$

$$\hat{X}_{n+1} = \bar{X}_n + \bar{\dot{X}}\ T$$

where

$\bar{X}_n$ = smooth position at time n

$\hat{X}_n$ = predicted position at time n

X_n = raw measured position

T = Sample interval

$\bar{\dot{X}}_n$ = smoothed velocity at time n

g and h = filter parameters.

These three equations reduce to:

$$\hat{X}_{n+1} = X_n (g + h) - g X_{n-1} + (2-g-h) \hat{X}_n - (1 - g) \hat{X}_{n-1} \quad .$$

If the output is considered $\hat{X}_{n+1}$ and the input is X_n, then the z transform is

$$H(z) = \frac{(g + h)z^2 - gz}{z^2 - (2-g-h)z + (1 - g)} \quad .$$

Because the predicted value is always used for the next measurement calculation a one period delay must be included. Therefore H(z) becomes

$$H(z) = \frac{(g + h)z - g}{z^2 - (2-g-h)z + (1 - g)} \quad .$$

This is the expression used in the analysis.

To simplify the analysis the block diagram was reduced to standard form. Note that an all sampled data system is assumed.

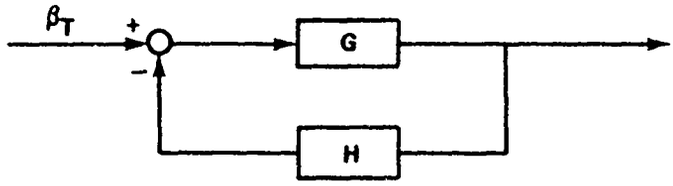

where $G = G_1 \frac{G_2}{1 - HG_2}$.

The characteristic equation of the system then becomes

$$1 - G_2H + G_1G_2 H = 0 \quad .$$

The numerator of this expression is the only part of interest and after combination becomes

$$z^2 + (Kg + Kh - 2)z + (1 - Kg) = 0 \quad .$$

Transformation to r - space, $z = \frac{r + 1}{r - 1}$ gives

$$Kh\ r^2 + 2Kg\ r + (4 - 2Kg - Kh) = 0 \quad .$$

For stability all poles must be in the left half-plane, so all coefficients above must have the same sign. For positive K the first two coefficients are always positive, so from the r^o coefficient

$$K < \frac{4}{2g + h} \quad .$$

This stability requirement is plotted on page 14 .

The k must now be related to the radar system parameters. From the simulation:

$$\beta_\epsilon = (SLP) \left(\frac{\Delta(\beta)}{\Sigma(\beta)}\right)$$

where Δ/Σ is the ratio of difference to sum channel voltages.

1) For antenna 1

$$\Delta(\beta) = \frac{\sin\left(P_1\beta - P_1P_3\right)}{\sin\left(P_2\beta - P_2P_3\right)} - \frac{\sin\left(P_1\beta + P_1P_3\right)}{\sin\left(P_2\beta + P_2P_3\right)}$$

$$\Sigma(\beta) = \frac{\sin\left(P_1\beta - P_1P_3\right)}{\sin\left(P_2\beta - P_2P_3\right)} + \frac{\sin\left(P_1\beta + P_1P_3\right)}{\sin\left(P_2\beta + P_2P_3\right)} \quad ,$$

where

$$P_1 = \frac{N\pi s}{\lambda}$$

$$P_2 = \frac{\pi s}{\lambda}$$

$$P_3 = \frac{\lambda}{2Ns}$$

N = number of elements per row or column

s = element spacing for rectangular array

λ = wavelength.

By the use of trigonometric identities the $\frac{\Delta}{\Sigma}$ using the above reduces to

$$\frac{\Delta(\beta)}{\Sigma(\beta)} = \cot\left(\frac{\pi}{2N}\right) \tan\left(P_2\beta\right)$$

and for the parameters used in this case

$$\frac{\Delta(\beta)}{\Sigma(\beta)} = 45.8 \tan(1.8\,\beta) \approx 82.5\,\beta \quad .$$

The small angle approximation may be justified since no discontinuity occurs in the region of interest, and a good straight line fit is possible. Thus

$$\frac{\Delta}{\Sigma} = k_1\beta \quad , \quad k_1 = 82.5$$

and for proper interpretation of the measurement

$$SLP = k_2 = \frac{1}{k_1} \quad .$$

This gives the general and specific expressions for the transfer function:

$$K = k_1 k_2 \quad , \quad k_1 = 82.5 \quad , \quad k_2 = 0.01208 \quad .$$

2) For Antenna 2 a closed form expression could not easily be derived, so the curve was evaluated numerically and the results shown in Figure B-1. The curve for Antenna I is also shown for comparison. An interesting and very practical problem arises when the value for k_2 is selected. If the slope (k_1) is measured at $\beta = 0$, then $k_2 = 0.02360$ radian/volt/volt. However, as indicated on the figure, this may not be as good as the value sometimes used by passing a line through the origin and the 1-degree point and using this slope, in this case, $k_2 = 0.01630$ radian/volt/volt.

Several simulation runs were made and the stability criteria presented in this case verified.

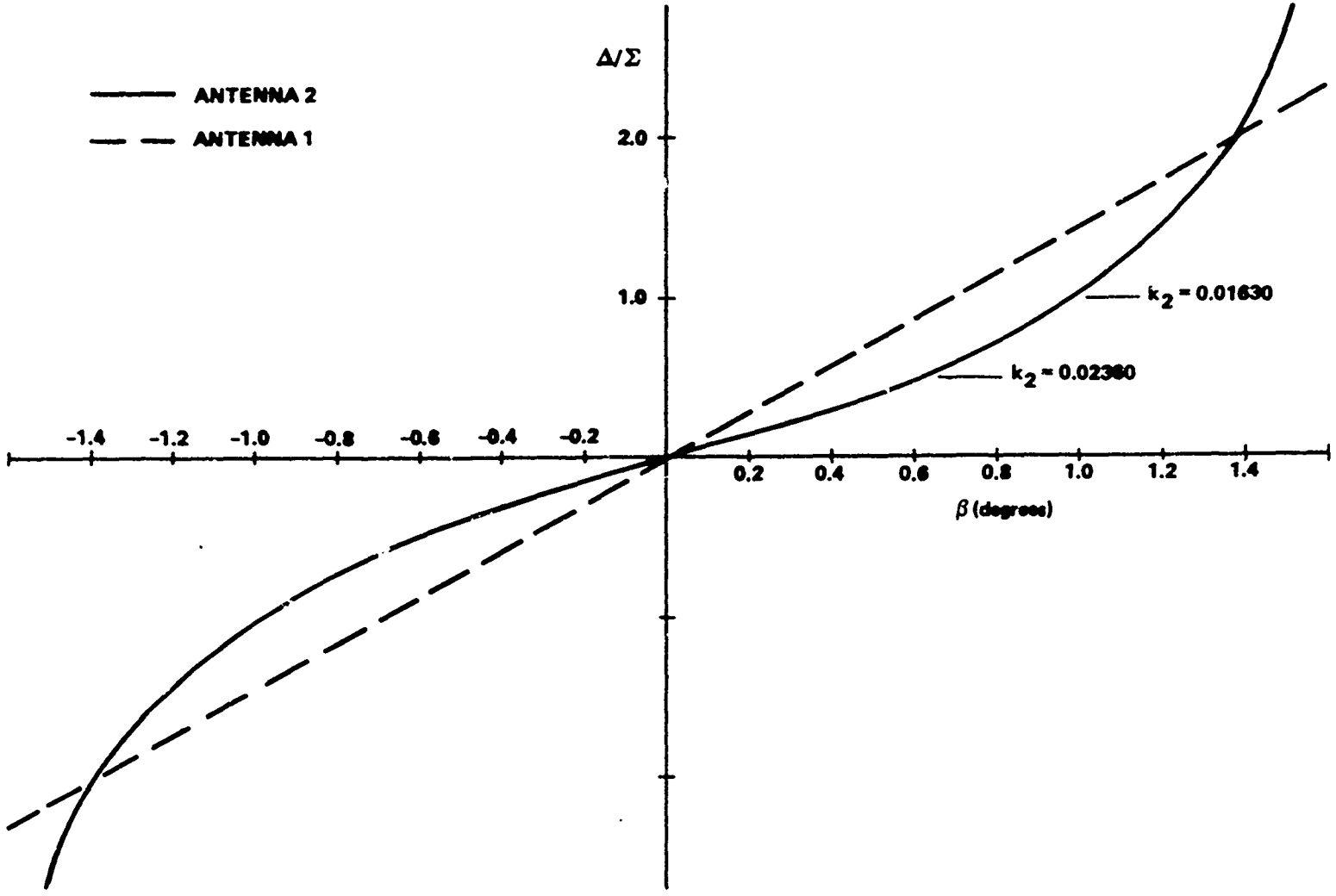

Figure B-1. Δ/Σ Curves